Structural reliability analysis by line sampling: A Bayesian active learning treatment

Chao Dang[a,*], Marcos A. Valdebenito[b], Matthias G.R. Faes[b], Jingwen Song[c], Pengfei Wei[d], Michael Beer[a,e,f]

[a] *Institute for Risk and Reliability, Leibniz University Hannover, Callinstr. 34, Hannover 30167, Germany*
[b] *Chair for Reliability Engineering, TU Dortmund University, Leonhard-Euler-Str. 5, Dortmund 44227, Germany*
[c] *School of Mechanical Engineering, Northwestern Polytechnical University, Xi'an 710072, PR China*
[d] *School of Power and Energy, Northwestern Polytechnical University, Xi'an 710072, PR China*
[e] *Institute for Risk and Uncertainty, University of Liverpool, Liverpool L69 7ZF, United Kingdom*
[f] *International Joint Research Center for Resilient Infrastructure & International Joint Research Center for Engineering Reliability and Stochastic Mechanics, Tongji University, Shanghai 200092, PR China*

Abstract

Line sampling has been demonstrated to be a promising simulation method for structural reliability analysis, especially for assessing small failure probabilities. However, its practical performance can still be significantly improved by taking advantage of, for example, Bayesian active learning. Along this direction, a recently proposed 'partially Bayesian active learning line sampling' (PBAL-LS) method has shown to be successful. This paper aims at offering a more complete Bayesian active learning treatment of line sampling, resulting in a new method called 'Bayesian active learning line sampling' (BAL-LS). Specifically, we derive the exact posterior variance of the failure probability, which can measure our epistemic uncertainty about the failure probability more precisely than the upper bound given in PBAL-LS. Further, two essential components (i.e., learning function and stopping criterion) are proposed to facilitate Bayesian active learning, based on the uncertainty representation of the failure probability. In addition, the important direction can be automatically updated throughout the simulation, as one advantage directly inherited from PBAL-LS. The performance of BAL-LS is illustrated by four numerical examples. It is shown that the proposed method is capable of evaluating extremely small failure probabilities with desired efficiency and accuracy.

Keywords:

Structural reliability analysis, Line sampling, Bayesian active learning, Bayesian inference, Gaussian process

1. Introduction

Structural reliability analysis usually involves calculating the complement of the so-called reliability of a structure or component, that is the failure probability P_f, which is formulated as a multiple integral:

$$P_f = \int_{\mathcal{X}} I(g(\boldsymbol{x})) f_{\boldsymbol{X}}(\boldsymbol{x}) \mathrm{d}\boldsymbol{x}, \tag{1}$$

where $\boldsymbol{X} = [X_1, X_2, \cdots, X_d]^{\mathrm{T}} \in \mathcal{X} \subseteq \mathbb{R}^d$ denotes a set of d basic random variables with known joint probability density function (PDF) $f_{\boldsymbol{X}}(\boldsymbol{x})$; $\boldsymbol{x} = [x_1, x_2, \cdots, x_d]^{\mathrm{T}}$ represents a realization of $\boldsymbol{X}$; $g(\cdot)$ is the limit state function (also known as performance function), which takes a value less than zero when a failure occurs; $I(\cdot)$ refers to the failure indicator function: $I(g(\boldsymbol{x})) = 1$ if $g(\boldsymbol{x}) < 0$ and $I(g(\boldsymbol{x})) = 0$ otherwise.

Except for some special cases, the failure probability integral, as defined in Eq. (1), is unlikely to be analytically solvable due largely to the underlying complexity of the limit state function (usually in an implicit form) in practice. Therefore, the development of efficient and accurate numerical methods to provide approximate solutions is of central interest from researchers and practitioners. Existing numerical methods for structural reliability analysis can be roughly divided into five categories [1]: stochastic simulation methods, asymptotic approximation methods, methods of moments, probability-conservation based methods and surrogate assisted methods. Among these categories, a prominent position is held by stochastic simulation techniques. They typically involve randomly simulating a large number of independent performance function values and then computing a failure probability estimate via an appropriate estimator. A non-exhaustive list of such techniques includes Monte Carlo simulation (MCS) [2], importance sampling [3, 4], directional sampling [5, 6], subset simulation [7, 8] and line sampling (LS) [9, 10]. As the most classic class of structural reliability analysis approaches, asymptotic approximation methods attempt to derive approximate solutions to the failure probability integral by using, e.g., Taylor series expansion. The most representative methods in this category are the first- and second order reliability methods (FORM, SORM) [11, 12]. The third category consists of methods of moments, in which the failure probability estimate is obtained by estimating

*Corresponding author
Email address: chao.dang@irz.uni-hannover.de (Chao Dang)

the probability distribution of the state variable (i.e., output variable of the performance function) or structural response of interest from the knowledge of its moments. In this context, the integer moments-based methods [13, 14] and fractional moments-based methods [15–17] are prevalent. As the fourth category, probability-conservation based methods also aim at capturing the probability distribution of the state variable or structural response, but build upon the principle of probability conservation. The probability density evolution method [18, 19] and direct probability integral method [20, 21] are two typical examples under this category. The search for more efficient and accurate methods for structural reliability analysis also promotes the development of surrogate assisted methods, especially combined with active learning. Examples of such methods include (but not limited to) efficient global reliability analysis [22] and active learning method combining Kriging and MCS (AK-MCS) [23]. For more information about surrogate assisted methods, one can refer to, e.g. [24, 25] and references therein. Despite those great efforts over the past several decades, no agreement has been reached so far on which method or kind of methods is better than others. In fact, each method has its own advantages and disadvantages. For practical applications, one should choose the most appropriate method considering the characteristics of both the problem at hand and the candidate reliability analysis methods.

In this study, we shall restrict our attention to LS. As a standard-alone stochastic simulation method, LS was originally developed by Koutsourelakis et al. [9]. The basic idea of it is to probe the failure domain using lines, rather than random points. Specifically, the failure probability is estimated by an average of the conditional failure probabilities corresponding to a set of random lines parallel to an important direction, which points towards the failure domain. LS has been demonstrated to be a promising stochastic simulation technique that is suitable for assessing small failure probabilities of weakly or moderately nonlinear reliability problems [26–29]. However, its performance strongly depends on three main aspects [30]:

(1) The important direction. A poor important direction will lead to a slow convergence rate of the subsequent MCS procedure, and hence unnecessary computational costs in order to achieve an acceptable result. On the contrary, an optimal importance direction is always desirable, which in turn requires a good knowledge about the limit state surface or many additional g-function evaluations.

(2) The numerical integrator. As a representative frequentist approach, the MCS method used in LS cannot make use of our prior knowledge on the limit state surface. Besides, it also shows a low convergence rate when an improper important direction is adopted and/or the limit surface around the important region is rough.

(3) The line search algorithm. To obtain each conditional failure probability, a root-finding algorithm is usually implemented. Therefore, the accuracy and efficiency of the selected root-finding algorithm also affect the overall performance of LS.

The traditional version of LS has been improved by several studies e.g., [31–33]. However, they still rely on the direct use of MCS, which can be less efficient, as discussed earlier. To further reduce the computational costs, there have been some research efforts to develop surrogate-assisted LS methods, e.g., metamodel LS [34] and adaptive Gaussian process regression-LS (AGPR-LS) [35]. More recently, the first author and his co-workers also proposed a partially Bayesian active learning LS (PBAL-LS) [30]. In PBAL-LS, estimation of the failure probability integral in LS is first interpreted as a Bayesian inference problem, where the posterior mean and an upper bound of the posterior variance for the failure probability are derived. Based on the uncertainty representation of the failure probability, a learning function and a stopping criterion that constitute two critical ingredients of active learning are then proposed to form the PBAL-LS method. Besides, the important direction in PBAL-LS can be updated on the fly throughout the simulation. To the best of knowledge of the authors, PBAL-LS is the first work that explores the Bayesian active learning (a concept originates from machine learning), at least partially, in the context of LS for structural reliability analysis.

The main objective of this work is to present a more complete Bayesian active learning treatment of LS. Specially, a full expression of the posterior variance of the failure probability in LS is deduced, which can measure our uncertainty about the failure probability more precisely than the upper bound given in [30]. The variance amplified importance sampling (VAIS) originally developed in [36] is introduced to approximate the posterior mean and variance of the failure probability, due to their analytical intractability. Based on the posterior statistics of the failure probability, we further propose a stopping criterion and a learning function

to enable active learning. Besides, some advantages of PBAL-LS are also inherited, e.g., the adaption of importance direction. We shall refer to this new development as Bayesian active learning LS (BAL-LS). It is expected that the proposed BAL-LS method can address the challenge of assessing (extremely) small failure probabilities for a class of weakly to moderately nonlinear problems in low to moderate dimensions.

The remaining of this paper is structured as follows. In Section 2, a general overview of several existing LS methods is given, among which two methods, i.e., standard LS and PBAL-LS, are briefly introduced. Section 3 presents the proposed BAL-LS method in detail. Four numerical examples are investigated in Section 4 to demonstrate the proposed method. Some concluding remarks are given in Section 5.

2. Literature review

This section first provides a general overview of several existing LS methods in the literature. Then, two of them, which are closely related to the proposed method, are briefly introduced.

2.1. General overview

LS has received a lot of attention from the structural reliability analysis community since its inception. This has led to the development of many variants of the traditional LS. We will not cover all of them, but only select some of the most important developments. The selected methods include the traditional LS [9], slime mold algorithm-assisted LS (LS-SMA) [37], advanced LS [31], adaptive LS [32], combination LS [33], multidomain LS [38], optimized LS [39], metamodel LS [34], AGPR-LS [35] and PBAL-LS [30]. They are compared in Table 1 regarding the important direction, numerical integrator and line search algorithm. Several aspects are worth mentioning:

- Multidomain LS allows for several important directions, while it is only applicable to a special class of series systems involving components whose response is linear with respect to a set of Gaussian random variables;
- Optimized LS adopts the ANN regression model as a surrogate of the original system model code, which is used only at the stage of determining the important direction. The failure probability is

finally obtained by using the direct MCS (LHS);

- Metamodel LS formulates the failure probability estimate as a product of a metamodel-based failure probability and a correction coefficient. The former is computed from a properly-trained Kriging model, while the latter is obtained from both the Kriging model and the original performance function;

- Overall, existing LS methods are only suitable or advantageous for a certain kind of problems with weak to moderate non-linearity.

Table 1: Comparison of several selected LS methods for structural reliability analysis.

Method	Important direction			Numerical integrator		Line search algorithm
	Multiple?	Adaptive?	Method	Direct MCS?	MCS on surrogate?	
Traditional LS [9]	✗	✗	MCMC	✓	✗	Not reported
LS-SMA [37]	✗	✗	FORM	✓	✗	SOPI
Advanced LS [31]	✗	✓(see [31])	Gradient (initial)	✓	✗	Newton's method
Adaptive LS [32]	✗	✓(see [32])	Not reported	✓	✗	Not reported
Combination LS [33]	✗	✓(see [33])	Gradient (initial)	✓	✗	Not reported
Multidomain LS [38]	✓(see [38])	✗	Analytical	✓	✗	See [38]
Optimized LS [39]	✗	✗	ANN assisted	✓(LHS)	✗	Not reported
Metamodel LS [34]	✗	✗	Gradient	✓	✓(Kriging)	Not reported
AGPR-LS [35]	✗	✗	FORM	✗	✓(GP)	SOPI
PBAL-LS [30]	✗	✓(see [30])	Gradient (initial)	✗	✓(GP)	Newton's method

MCMC = Markov chain Monte Carlo; SOPI = second-order polynomial interpolation; FORM = first-order reliability method; ANN = artificial neural network; LHS = Latin hypercube sampling; GP = Gaussian process

2.2. Brief review of two related methods

2.2.1. Traditional line sampling

The failure probability integral defined in Eq. (1) can be reformulated in the standard normal space such that:

$$P_f = \int_{\mathcal{U}} I(\mathcal{G}(\boldsymbol{u}))\phi_{\boldsymbol{U}}(\boldsymbol{u})\mathrm{d}\boldsymbol{u}, \tag{2}$$

where $\boldsymbol{U} = [U_1, U_2, \cdots, U_d]^{\mathrm{T}} \in \mathcal{U} \subseteq \mathbb{R}^d$ is a vector of d i.i.d. standard normal variables with joint PDF $\phi_{\boldsymbol{U}}(\boldsymbol{u}) = (2\pi)^{-d/2}\exp(-\boldsymbol{u}^{\mathrm{T}}\boldsymbol{u}/2)$; $\boldsymbol{u} = [u_1, u_2, \cdots, u_d]^{\mathrm{T}}$ denotes a random realization of $\boldsymbol{U}$; $\mathcal{G} = g \circ T^{-1}$ can be called a transformed limit state function; $T : \mathcal{X} \to \mathcal{U}$ represents an appropriate operator that can transform $\boldsymbol{X}$ to $\boldsymbol{U}$, e.g., an isoprobabilistic transformation.

The formulation of the traditional LS method relies on the assumption that an important direction $\boldsymbol{\alpha}$ can be identified, which is a unit vector pointing towards the failure domain $F = \{\boldsymbol{u} \in \mathcal{U} : \mathcal{G}(\boldsymbol{u}) < 0\}$, as shown in Fig. 1. Once $\boldsymbol{\alpha}$ is given, the d-dimensional standard normal vector $\boldsymbol{U}$ can be expressed in a rotated coordinate system such that:

$$\boldsymbol{U} = \boldsymbol{R}\boldsymbol{U}' = \boldsymbol{\alpha}U^{\parallel} + \boldsymbol{Q}\boldsymbol{U}^{\perp}, \tag{3}$$

where $\boldsymbol{R}$ is a $d \times d$ rotational matrix with its first row being $\boldsymbol{\alpha}^{\mathrm{T}}$ and the rest rows being $\boldsymbol{Q}^{\mathrm{T}}$; $\boldsymbol{Q}$ is a $d \times (d-1)$ matrix containing $d-1$ orthogonal basis vectors of the hyperplane perpendicular to $\boldsymbol{\alpha}$; $\boldsymbol{U}' = [U^{\parallel}, \boldsymbol{U}^{\perp\mathrm{T}}]^{\mathrm{T}} \in \mathcal{U}' \subseteq \mathbb{R}^d$ is a d-dimensional rotated standard normal vector of $\boldsymbol{U}$, due to the rotational invariance of standard normal vector; $U^{\parallel} \in \mathcal{U}^{\parallel} \subseteq \mathbb{R}$ is a standard normal variable, while $\boldsymbol{U}^{\perp} = [U_1^{\perp}, U_2^{\perp}, \cdots, U_{d-1}^{\perp}]^{\mathrm{T}} \in \mathcal{U}^{\perp} \subseteq \mathbb{R}^{d-1}$ is a $(d-1)$-dimensional standard normal vector.

It follows that the failure probability integral defined in Eq. (2) can be reformulated as:

$$\begin{aligned}
P_f &= \int_{\mathcal{U}'} I(\mathcal{G}(\boldsymbol{R}\boldsymbol{u}'))\phi_{\boldsymbol{U}'}(\boldsymbol{u}')\mathrm{d}\boldsymbol{u}' \\
&= \int_{\mathcal{U}^{\perp}} \int_{\mathcal{U}^{\parallel}} I(\mathcal{G}(\boldsymbol{\alpha}u^{\parallel} + \boldsymbol{Q}\boldsymbol{u}^{\perp}))\phi_{U^{\parallel}}(u^{\parallel})\phi_{\boldsymbol{U}^{\perp}}(\boldsymbol{u}^{\perp})\mathrm{d}u^{\parallel}\mathrm{d}\boldsymbol{u}^{\perp} \\
&= \int_{\mathcal{U}^{\perp}} \left(\int_{\mathcal{U}^{\parallel}} I(\mathcal{G}(\boldsymbol{\alpha}u^{\parallel} + \boldsymbol{Q}\boldsymbol{u}^{\perp}))\phi_{U^{\parallel}}(u^{\parallel})\mathrm{d}u^{\parallel} \right) \phi_{\boldsymbol{U}^{\perp}}(\boldsymbol{u}^{\perp})\mathrm{d}\boldsymbol{u}^{\perp} \\
&= \int_{\mathcal{U}^{\perp}} p(\boldsymbol{u}^{\perp})\phi_{\boldsymbol{U}^{\perp}}(\boldsymbol{u}^{\perp})\mathrm{d}\boldsymbol{u}^{\perp},
\end{aligned} \tag{4}$$

where $\phi_{U^{\parallel}}(u^{\parallel})$ and $\phi_{\boldsymbol{U}^{\perp}}(\boldsymbol{u}^{\perp})$ are the (joint) PDF of $U^{\parallel}$ and $\boldsymbol{U}^{\perp}$; $p(\boldsymbol{u}^{\perp}) = \int_{\mathcal{U}^{\parallel}} I(\mathcal{G}(\boldsymbol{\alpha}u^{\parallel} + \boldsymbol{Q}\boldsymbol{u}^{\perp}))\phi_{U^{\parallel}}(u^{\parallel})\mathrm{d}u^{\parallel}$ can be interpreted as a conditional failure probability given $\boldsymbol{U}^{\perp} = \boldsymbol{u}^{\perp}$, which is associated with a one-dimensional reliability problem with performance function $\mathcal{G}(\boldsymbol{\alpha}U^{\parallel} + \boldsymbol{Q}\boldsymbol{u}^{\perp})$. In case that the failure domain F is a simple half-open domain (as shown in Fig. 1), the conditional failure probability $p(\boldsymbol{u}^{\perp})$ is equal to:

$$p(\boldsymbol{u}^{\perp}) = \Phi(-\beta(\boldsymbol{u}^{\perp})), \tag{5}$$

where Φ denotes the cumulative distribution function of the standard normal variable; $\beta(\boldsymbol{u}^{\perp})$ is the Euclidean distance between $\boldsymbol{u}^{\perp}$ and the limit state surface $\mathcal{G}(\boldsymbol{u}) = 0$ along the direction $\boldsymbol{\alpha}$. Using Eq. (5), Eq. (4) is simplified as:

$$P_f = \int_{\mathcal{U}^{\perp}} \Phi(-\beta(\boldsymbol{u}^{\perp}))\phi_{\boldsymbol{U}^{\perp}}(\boldsymbol{u}^{\perp})\mathrm{d}\boldsymbol{u}^{\perp}, \tag{6}$$

Note that Eq. (6) rather than Eq. (4) is commonly considered in the traditional LS method, and also other improved LS methods.

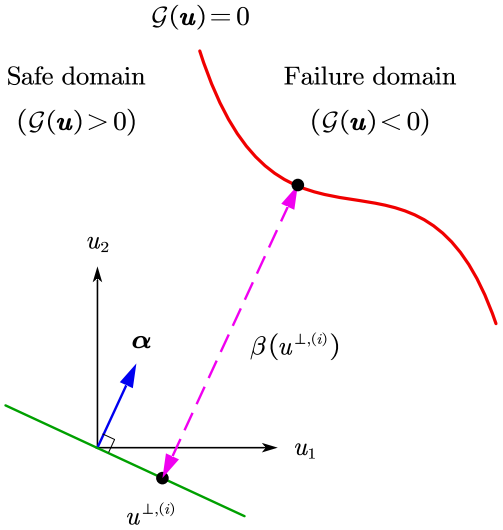

Figure 1: Schematic illustration of traditional LS in two dimensions.

In the traditional LS method, the failure probability integral defined in Eq. (6) is solved by the MCS method in conjunction with a root-finding technique. A MCS estimator of P_f is given by:

$$\hat{P}_f = \frac{1}{N}\sum_{i=1}^{N} \Phi(-\beta(\boldsymbol{u}^{\perp,(i)})), \tag{7}$$

where $\left\{\boldsymbol{u}^{\perp,(i)}\right\}_{i=1}^{N}$ is a set of N random samples generated according to $\phi_{\boldsymbol{U}^{\perp}}(\boldsymbol{u}^{\perp})$. For each sample $\boldsymbol{u}^{\perp,(i)}$, $\beta(\boldsymbol{u}^{\perp,(i)})$ is considered as the solution of $u^{\parallel}$ subject to $\mathcal{G}(\boldsymbol{\alpha}u^{\parallel}+\boldsymbol{Q}\boldsymbol{u}^{\perp,(i)})=0$ (as illustrated in Fig. 1), which can be solved by a suitable root-finding algorithm. The variance associated with $\hat{P}_f$ can be estimated by:

$$\mathrm{Var}\left[\hat{P}_f\right]=\frac{1}{N(N-1)}\sum_{i=1}^{N}\left(\Phi(-\beta(\boldsymbol{u}^{\perp,(i)}))-\hat{P}_f\right)^2. \tag{8}$$

2.2.2. Partially Bayesian active learning line sampling

PBAL-LS [30] offers a Bayesian active learning alternative to the traditional LS method and its variants. Specifically, the task of estimating the failure probability integral defined in Eq. (6) is first interpreted as a Bayesian inference problem. Then, such a task is further framed in an active learning setting based on the posterior statistics of the failure probability. Besides, another notable feature of PBAL-LS is that the importance direction needs not to be optimal at the very beginning, and it can be updated on the fly through the simulation.

PBAL-LS begins by modeling our uncertainty over the β-function with a Gaussian process (GP):

$$\tilde{\beta}_0(\boldsymbol{u}^{\perp})\sim\mathcal{GP}(m_{\tilde{\beta}_0}(\boldsymbol{u}^{\perp}),k_{\tilde{\beta}_0}(\boldsymbol{u}^{\perp},\boldsymbol{u}^{\perp\prime})), \tag{9}$$

where $\tilde{\beta}_0$ represents the prior distribution of β before seeing any observations; $m_{\tilde{\beta}_0}(\boldsymbol{u}^{\perp})$ and $k_{\tilde{\beta}_0}(\boldsymbol{u}^{\perp},\boldsymbol{u}^{\perp\prime})$ are the prior mean and covariance functions, which are specified as a constant value and square exponential kernel [30], respectively.

Suppose that now we have an observation matrix $\boldsymbol{\mathcal{D}}=\left\{\boldsymbol{\mathcal{U}}^{\perp},\boldsymbol{\mathcal{Y}}\right\}$, where $\boldsymbol{\mathcal{U}}^{\perp}=\left\{\boldsymbol{u}^{\perp,(i)}\right\}_{i=1}^{n}$ is a $(d-1)\times n$ matrix consisting of n observed locations on the hyperplane orthogonal to the important direction, and $\boldsymbol{\mathcal{Y}}=\left\{y^{(i)}\right\}_{i=1}^{n}$ is an $n\times 1$ vector with $y^{(i)}=\beta(\boldsymbol{u}^{\perp,(i)})$. Conditioning on data $\boldsymbol{\mathcal{D}}$, the posterior distribution of β turns out to be another GP of the form:

$$\tilde{\beta}_n(\boldsymbol{u}^{\perp})\sim\mathcal{GP}(m_{\tilde{\beta}_n}(\boldsymbol{u}^{\perp}),k_{\tilde{\beta}_n}(\boldsymbol{u}^{\perp},\boldsymbol{u}^{\perp\prime})), \tag{10}$$

where $\tilde{\beta}_n$ denotes the posterior distribution of β conditional on n observations; $m_{\tilde{\beta}_n}(\boldsymbol{u}^{\perp})$ and $k_{\tilde{\beta}_n}(\boldsymbol{u}^{\perp},\boldsymbol{u}^{\perp\prime})$ are respectively the posterior mean and covariance functions, which can be expressed in closed form [40]:

$$m_{\tilde{\beta}_n}(\boldsymbol{u}^{\perp})=m_{\tilde{\beta}_0}(\boldsymbol{u}^{\perp})+\boldsymbol{k}_{\beta_0}(\boldsymbol{u}^{\perp},\boldsymbol{\mathcal{U}}^{\perp})^{\mathrm{T}}\boldsymbol{K}_{\beta_0}(\boldsymbol{\mathcal{U}}^{\perp},\boldsymbol{\mathcal{U}}^{\perp})^{-1}(\boldsymbol{\mathcal{Y}}-\boldsymbol{m}_{\tilde{\beta}_0}(\boldsymbol{\mathcal{U}}^{\perp})), \tag{11}$$

$$k_{\tilde{\beta}_n}(\boldsymbol{u}^{\perp},\boldsymbol{u}^{\perp\prime}) = k_{\tilde{\beta}_0}(\boldsymbol{u}^{\perp},\boldsymbol{u}^{\perp\prime}) - \boldsymbol{k}_{\beta_0}(\boldsymbol{u}^{\perp},\boldsymbol{\mathcal{U}}^{\perp})^{\mathrm{T}}\boldsymbol{K}_{\beta_0}(\boldsymbol{\mathcal{U}}^{\perp},\boldsymbol{\mathcal{U}}^{\perp})^{-1}\boldsymbol{k}_{\beta_0}(\boldsymbol{\mathcal{U}}^{\perp},\boldsymbol{u}^{\perp\prime}), \tag{12}$$

where $\boldsymbol{m}_{\tilde{\beta}_0}(\boldsymbol{\mathcal{U}}^{\perp})$ is an n-by-1 mean vector whose i-th element is $m_{\tilde{\beta}_0}(\boldsymbol{u}^{\perp,(i)})$; $\boldsymbol{k}_{\beta_0}(\boldsymbol{u}^{\perp},\boldsymbol{\mathcal{U}}^{\perp})$ is an n-by-1 covariance vector whose i-th entry is $k_{\tilde{\beta}_0}(\boldsymbol{u}^{\perp},\boldsymbol{u}^{\perp,(i)})$; $\boldsymbol{k}_{\beta_0}(\boldsymbol{\mathcal{U}}^{\perp},\boldsymbol{u}^{\perp\prime})$ is an n-by-1 covariance vector whose i-th entry is $\boldsymbol{k}_{\beta_0}(\boldsymbol{u}^{\perp,(i)},\boldsymbol{u}^{\perp\prime})$; $\boldsymbol{K}_{\beta_0}(\boldsymbol{\mathcal{U}}^{\perp},\boldsymbol{\mathcal{U}}^{\perp})$ is an n-by-n covariance matrix with (i,j)-th entry being $k_{\beta_0}(\boldsymbol{u}^{\perp,(i)},\boldsymbol{u}^{\perp,(j)})$.

Through some mathematical derivations, we can arrive at the posterior mean and an upper bound of posterior variance for the failure probability [30]:

$$m_{\tilde{P}_{f,n}} = \int_{\mathbb{R}^{d-1}} \Phi\left(\frac{-m_{\tilde{\beta}_n}(\boldsymbol{u}^{\perp})}{\sqrt{1+\sigma^2_{\tilde{\beta}_n}(\boldsymbol{u}^{\perp})}}\right)\phi_{\boldsymbol{U}^{\perp}}(\boldsymbol{u}^{\perp})\mathrm{d}\boldsymbol{u}^{\perp}, \tag{13}$$

$$\overline{\sigma}^2_{\tilde{P}_{f,n}} = \left(\int_{\mathbb{R}^{d-1}} \sqrt{\Phi\left(\frac{-m_{\tilde{\beta}_n}(\boldsymbol{u}^{\perp})}{\sqrt{1+\sigma^2_{\tilde{\beta}_n}(\boldsymbol{u}^{\perp})}}\right)\Phi\left(\frac{m_{\tilde{\beta}_n}(\boldsymbol{u}^{\perp})}{\sqrt{1+\sigma^2_{\tilde{\beta}_n}(\boldsymbol{u}^{\perp})}}\right) - 2\mathcal{T}\left(\frac{-m_{\tilde{\beta}_n}(\boldsymbol{u}^{\perp})}{\sqrt{1+\sigma^2_{\tilde{\beta}_n}(\boldsymbol{u}^{\perp})}}, \frac{1}{\sqrt{1+2\sigma^2_{\tilde{\beta}_n}(\boldsymbol{u}^{\perp})}}\right)} \times\phi_{\boldsymbol{U}^{\perp}}(\boldsymbol{u}^{\perp})\mathrm{d}\boldsymbol{u}^{\perp}\right)^2, \tag{14}$$

where $\sigma^2_{\tilde{\beta}_n}(\boldsymbol{u}^{\perp})$ is the posterior variance function of β, i.e., $\sigma^2_{\tilde{\beta}_n}(\boldsymbol{u}^{\perp}) = k_{\tilde{\beta}_n}(\boldsymbol{u}^{\perp},\boldsymbol{u}^{\perp})$; $\mathcal{T}(\cdot,\cdot)$ is the Owen's T function. The posterior mean $m_{\tilde{P}_{f,n}}$ can be used naturally as the failure probability estimate, while the upper bound of posterior variance $\overline{\sigma}^2_{\tilde{P}_{f,n}}$ measures our maximum uncertainty about the estimate.

On the basis of Eq. (14), a learning function, called 'upper-bound posterior standard deviation contribution' (UPSDC), is proposed in [30]:

$$\mathrm{UPSDC}(\boldsymbol{u}^{\perp}) = \sqrt{\Phi\left(\frac{-m_{\tilde{\beta}_n}(\boldsymbol{u}^{\perp})}{\sqrt{1+\sigma^2_{\tilde{\beta}_n}(\boldsymbol{u}^{\perp})}}\right)\Phi\left(\frac{m_{\tilde{\beta}_n}(\boldsymbol{u}^{\perp})}{\sqrt{1+\sigma^2_{\tilde{\beta}_n}(\boldsymbol{u}^{\perp})}}\right) - 2\mathcal{T}\left(\frac{-m_{\tilde{\beta}_n}(\boldsymbol{u}^{\perp})}{\sqrt{1+\sigma^2_{\tilde{\beta}_n}(\boldsymbol{u}^{\perp})}}, \frac{1}{\sqrt{1+2\sigma^2_{\tilde{\beta}_n}(\boldsymbol{u}^{\perp})}}\right)} \times\phi_{\boldsymbol{U}^{\perp}}(\boldsymbol{u}^{\perp}). \tag{15}$$

Note that $\overline{\sigma}_{\tilde{P}_{F,n}} = \int_{\mathbb{R}^{d-1}} \mathrm{UPSDC}(\boldsymbol{u}^{\perp})\,\mathrm{d}\boldsymbol{u}^{\perp}$ holds. In case that the prescribed stopping criterion is not satisfied, the best next point is then selected by maximizing the UPSDC function, i.e., $\boldsymbol{u}^{\perp,(n+1)} = \arg\max_{\boldsymbol{u}^{\perp}\in\mathcal{U}^{\perp}} \mathrm{UPSDC}(\boldsymbol{u}^{\perp})$. In PBAL-LS, the stopping criterion is defined based on judging the upper bound of the posterior coefficient of variation of the failure probability [30]:

$$\overline{\mathrm{COV}}_{\tilde{P}_{f,n}} = \frac{\overline{\sigma}_{\tilde{P}_{f,n}}}{m_{\tilde{P}_{f,n}}} < \epsilon, \tag{16}$$

where ϵ is a user-specified tolerance.

The interested reader is referred to [30] for theoretical and algorithmic details of PBAL-LS. It is shown that PBAL-LS outperforms most, if not all, of the existing LS methods for several benchmark problems. Despite this, PBAL-LS still belongs to a kind of PBAL method largely due to unavailability of the posterior variance for the failure probability, and a complete Bayesian active learning treatment is worth studying. The main reasons are the following. First, the upper bound of the posterior variance for the failure probability (Eq. (14)) might be too loose to reflect our real epistemic uncertainty about the failure probability estimate. In addition, it is difficult and even impossible for us to know to what extent the real epistemic uncertainty is magnified when using Eq. (14). Second, the learning function (i.e., the UPSDC function defined in Eq. (15)) could be less effective because it comes from the upper bound of the posterior variance of the failure probability (Eq. (14)), which is the result of a very strict assumption. Third, it is difficult to specify a proper tolerance ϵ (that is related to the true posterior COV of the failure probability) for the stopping criterion. A conservative choice is to set a small ϵ, which may lead to an accurate estimate for the failure probability, but usually causes unnecessary computational costs.

3. Bayesian active learning line sampling

In the present section, BAL-LS as an enhanced version of the previously developed PBAL-LS is introduced. First, the posterior mean and variance of the failure probability defined in Eq. (6) are devised so as to offer a more complete Bayesian interpretation of the standard LS. The approximate solutions for the posterior mean and variance are also given, due to their analytical intractability. Based on the posterior statistics of the failure probability, two principal elements, i.e., learning function and stopping criterion, are proposed, which enables us to offer a new Bayesian active learning treatment for the standard LS. Finally, the numerical implementation procedure of BAL-LS is summarized, where how to adapt the important direction and process each line are explained.

3.1. Posterior mean and variance of the failure probability

Proposition 1. *If a GP prior is assigned to the β-function (i.e., Eq. (9)), the posterior mean and variance of the failure probability defined in Eq. (6) can be expressed as:*

$$m_{\tilde{P}_{f,n}} = \int_{\mathcal{U}^\perp} m_{\tilde{\Phi}_n(-\tilde{\beta})}\left(\boldsymbol{u}^\perp\right) \phi_{\boldsymbol{U}^\perp}(\boldsymbol{u}^\perp)\mathrm{d}\boldsymbol{u}^\perp, \tag{17}$$

$$\sigma^2_{\tilde{P}_{f,n}} = \int_{\mathcal{U}^\perp}\int_{\mathcal{U}^\perp} k_{\tilde{\Phi}_n(-\tilde{\beta})}(\boldsymbol{u}^\perp, \boldsymbol{u}^{\perp\prime})\phi_{\boldsymbol{U}^\perp}(\boldsymbol{u}^\perp)\phi_{\boldsymbol{U}^{\perp\prime}}(\boldsymbol{u}^{\perp\prime})\mathrm{d}\boldsymbol{u}^\perp\mathrm{d}\boldsymbol{u}^{\perp\prime} \tag{18}$$

where $m_{\tilde{\Phi}_n(-\tilde{\beta})}\left(\boldsymbol{u}^\perp\right)$ and $k_{\tilde{\Phi}_n(-\tilde{\beta})}(\boldsymbol{u}^\perp, \boldsymbol{u}^{\perp\prime})$ are the posterior mean and covariance functions of $\Phi(-\beta)$.

Proof. Analogy to our previous results (see Eqs. (23) and (24) in [36]), the above proposition is easy to be proved by using the Fubini's theorem. Therefore, the detailed proof is omitted here. □

3.1.1. Posterior mean of the failure probability

Proposition 2. *If a GP prior is placed over the β-function (i.e., Eq. (9)), the posterior mean function of $\Phi(-\beta)$ takes the form:*

$$m_{\tilde{\Phi}_n(-\tilde{\beta})}\left(\boldsymbol{u}^\perp\right) = \Phi\left(\frac{-m_{\tilde{\beta}_n}\left(\boldsymbol{u}^\perp\right)}{\sqrt{1+\sigma^2_{\tilde{\beta}_n}\left(\boldsymbol{u}^\perp\right)}}\right). \tag{19}$$

Proof. The posterior mean function $m_{\tilde{\Phi}_n(-\tilde{\beta})}\left(\boldsymbol{u}^\perp\right)$ can be further written as:

$$\begin{aligned} m_{\tilde{\Phi}_n(-\tilde{\beta})}\left(\boldsymbol{u}^\perp\right) =& \mathbb{E}_{\tilde{\beta}_n}\left[\Phi(-\tilde{\beta}_n\left(\boldsymbol{u}^\perp\right))\right] \\ =& 1 - \int_{\infty}^{\infty} \Phi\left(-z\right) \frac{1}{\sigma_{\tilde{\beta}_n}\left(\boldsymbol{u}^\perp\right)} \phi\left(\frac{z - m_{\tilde{\beta}_n}\left(\boldsymbol{u}^\perp\right)}{\sigma_{\tilde{\beta}_n}\left(\boldsymbol{u}^\perp\right)}\right) \mathrm{d}z \\ =& 1 - \int_{-\infty}^{\infty} \Phi\left(m_{\tilde{\beta}_n}\left(\boldsymbol{u}^\perp\right) + \sigma_{\tilde{\beta}_n}\left(\boldsymbol{u}^\perp\right) v\right) \phi\left(v\right) \mathrm{d}v. \end{aligned} \tag{20}$$

Note that the following equation holds

$$\int_{-\infty}^{\infty} \Phi\left(m_{\tilde{\beta}_n}\left(\boldsymbol{u}^\perp\right) + \sigma_{\tilde{\beta}_n}\left(\boldsymbol{u}^\perp\right) v\right) \phi\left(v\right) \mathrm{d}v = \Phi\left(\frac{m_{\tilde{\beta}_n}\left(\boldsymbol{u}^\perp\right)}{\sqrt{1+\sigma^2_{\tilde{\beta}_n}\left(\boldsymbol{u}^\perp\right)}}\right), \tag{21}$$

which has been given repeatedly in the literature, with or without proof. One can refer to, e.g., [41], for a proof. Substituting Eq. (21) into Eq. (20), Eq. (19) can be proved.

□

Substituting Eq. (19) into Eq. (17), the posterior mean of the failure probability can be obtained as in Eq. (13).

3.1.2. Posterior variance of the failure probability

Proposition 3. *If a GP prior is assumed for the β-function (i.e., Eq. (9)), the posterior covariance function of $\Phi(-\beta)$ is formulated as:*

$$\begin{aligned} k_{\tilde{\Phi}_n(-\tilde{\beta})}(\boldsymbol{u}^{\perp},\boldsymbol{u}^{\perp\prime}) =& \mathcal{F}\left(\begin{bmatrix} m_{\tilde{\beta}_n}\left(\boldsymbol{u}^{\perp}\right) \\ m_{\tilde{\beta}_n}\left(\boldsymbol{u}^{\perp\prime}\right) \end{bmatrix}; \begin{bmatrix} 0 \\ 0 \end{bmatrix}, \begin{bmatrix} \sigma^2_{\tilde{\beta}_n}\left(\boldsymbol{u}^{\perp}\right)+1 & k_{\tilde{\beta}_n}(\boldsymbol{u}^{\perp},\boldsymbol{u}^{\perp\prime}) \\ k_{\tilde{\beta}_n}(\boldsymbol{u}^{\perp\prime},\boldsymbol{u}^{\perp}) & \sigma^2_{\tilde{\beta}_n}\left(\boldsymbol{u}^{\perp\prime}\right)+1 \end{bmatrix}\right) \\ & - \Phi\left(\frac{m_{\tilde{\beta}_n}\left(\boldsymbol{u}^{\perp}\right)}{\sqrt{1+\sigma^2_{\tilde{\beta}_n}\left(\boldsymbol{u}^{\perp}\right)}}\right)\Phi\left(\frac{m_{\tilde{\beta}_n}\left(\boldsymbol{u}^{\perp\prime}\right)}{\sqrt{1+\sigma^2_{\tilde{\beta}_n}\left(\boldsymbol{u}^{\perp\prime}\right)}}\right), \end{aligned} \tag{22}$$

where $\mathcal{F}$ denotes the bivariate Gaussian CDF, which does not have a closed form. Alternatively, it can be approximated by several existing numerical methods, e.g., [42].

Proof. The posterior covariance function $k_{\tilde{\Phi}_n(-\tilde{\beta})}(\boldsymbol{u}^{\perp},\boldsymbol{u}^{\perp\prime})$ is further expressed as:

$$\begin{aligned} k_{\tilde{\Phi}_n(-\tilde{\beta})}(\boldsymbol{u}^{\perp},\boldsymbol{u}^{\perp\prime}) =& \mathbb{E}_{\tilde{\beta}_n}\left[\left(\Phi\left(-\tilde{\beta}_n\left(\boldsymbol{u}^{\perp}\right)\right)-\mathbb{E}_{\tilde{\beta}_n}\left[\Phi\left(-\tilde{\beta}_n\left(\boldsymbol{u}^{\perp}\right)\right)\right]\right)\left(\Phi\left(-\tilde{\beta}_n\left(\boldsymbol{u}^{\perp\prime}\right)\right)-\mathbb{E}_{\tilde{\beta}_n}\left[\Phi\left(-\tilde{\beta}_n\left(\boldsymbol{u}^{\perp\prime}\right)\right)\right]\right)\right] \\ =& \mathbb{E}_{\tilde{\beta}_n}\left[\Phi\left(-\tilde{\beta}_n\left(\boldsymbol{u}^{\perp}\right)\right)\Phi\left(-\tilde{\beta}_n\left(\boldsymbol{u}^{\perp\prime}\right)\right)\right]-\mathbb{E}_{\tilde{\beta}_n}\left[\Phi\left(-\tilde{\beta}_n\left(\boldsymbol{u}^{\perp}\right)\right)\right]\mathbb{E}_{\tilde{\beta}_n}\left[\Phi\left(-\tilde{\beta}_n\left(\boldsymbol{u}^{\perp\prime}\right)\right)\right] \\ =& \mathbb{E}_{\tilde{\beta}_n}\left[\left(1-\Phi\left(\tilde{\beta}_n\left(\boldsymbol{u}^{\perp}\right)\right)\right)\left(1-\Phi\left(\tilde{\beta}_n\left(\boldsymbol{u}^{\perp\prime}\right)\right)\right)\right]-\mathbb{E}_{\tilde{\beta}_n}\left[1-\Phi\left(\tilde{\beta}_n\left(\boldsymbol{u}^{\perp}\right)\right)\right]\mathbb{E}_{\tilde{\beta}_n}\left[1-\Phi\left(\tilde{\beta}_n\left(\boldsymbol{u}^{\perp\prime}\right)\right)\right] \\ =& \mathbb{E}_{\tilde{\beta}_n}\left[\Phi\left(\tilde{\beta}_n\left(\boldsymbol{u}^{\perp}\right)\right)\Phi\left(\tilde{\beta}_n\left(\boldsymbol{u}^{\perp\prime}\right)\right)\right]-\mathbb{E}_{\tilde{\beta}_n}\left[\Phi\left(\tilde{\beta}_n\left(\boldsymbol{u}^{\perp}\right)\right)\right]\mathbb{E}_{\tilde{\beta}_n}\left[\Phi\left(\tilde{\beta}_n\left(\boldsymbol{u}^{\perp\prime}\right)\right)\right] \\ =& \int_{-\infty}^{\infty}\Phi\left(m_{\tilde{\beta}_n}\left(\boldsymbol{u}^{\perp}\right)+\sigma_{\tilde{\beta}_n}\left(\boldsymbol{u}^{\perp}\right)v\right)\Phi\left(m_{\tilde{\beta}_n}\left(\boldsymbol{u}^{\perp\prime}\right)+\sigma_{\tilde{\beta}_n}\left(\boldsymbol{u}^{\perp\prime}\right)w\right)\phi(v)\,\phi(w)\,\mathrm{d}v\mathrm{d}w \\ & -\Phi\left(\frac{m_{\tilde{\beta}_n}\left(\boldsymbol{u}^{\perp}\right)}{\sqrt{1+\sigma^2_{\tilde{\beta}_n}\left(\boldsymbol{u}^{\perp}\right)}}\right)\Phi\left(\frac{m_{\tilde{\beta}_n}\left(\boldsymbol{u}^{\perp\prime}\right)}{\sqrt{1+\sigma^2_{\tilde{\beta}_n}\left(\boldsymbol{u}^{\perp\prime}\right)}}\right), \end{aligned} \tag{23}$$

By making use of the result in [43], we have

$$\begin{aligned} & \int_{-\infty}^{\infty}\Phi\left(m_{\tilde{\beta}_n}\left(\boldsymbol{u}^{\perp}\right)+\sigma_{\tilde{\beta}_n}\left(\boldsymbol{u}^{\perp}\right)v\right)\Phi\left(m_{\tilde{\beta}_n}\left(\boldsymbol{u}^{\perp\prime}\right)+\sigma_{\tilde{\beta}_n}\left(\boldsymbol{u}^{\perp\prime}\right)w\right)\phi(v)\,\phi(w)\,\mathrm{d}v\mathrm{d}w \\ =& \mathcal{F}\left(\begin{bmatrix} m_{\tilde{\beta}_n}\left(\boldsymbol{u}^{\perp}\right) \\ m_{\tilde{\beta}_n}\left(\boldsymbol{u}^{\perp\prime}\right) \end{bmatrix}; \begin{bmatrix} 0 \\ 0 \end{bmatrix}, \begin{bmatrix} \sigma^2_{\tilde{\beta}_n}\left(\boldsymbol{u}^{\perp}\right)+1 & k_{\tilde{\beta}_n}(\boldsymbol{u}^{\perp},\boldsymbol{u}^{\perp\prime}) \\ k_{\tilde{\beta}_n}(\boldsymbol{u}^{\perp\prime},\boldsymbol{u}^{\perp}) & \sigma^2_{\tilde{\beta}_n}\left(\boldsymbol{u}^{\perp\prime}\right)+1 \end{bmatrix}\right). \end{aligned} \tag{24}$$

The proof of Eq. (24) is referred to the supplementary materials for [43]. Substituting Eq. (24) into Eq. (23), Eq. (22) can be proved.

□

The posterior variance of the failure probability can be obtained by substituting Eq. (22) into Eq. (18). It is worth mentioning that the upper bound of the posterior variance given in Eq. (14) can be obtained from Eq. (18) by using the Cauchy–Schwarz inequality for $k_{\tilde{\Phi}_n(-\tilde{\beta})}(\boldsymbol{u}^{\perp}, \boldsymbol{u}^{\perp\prime})$. Thus, the upper bound is achieved only when the posterior distribution of $\Phi(-\beta)$ between any two locations is linearly dependent. This condition is very strict and hence in most practical cases $\sigma^2_{\tilde{P}_{f,n}} < \overline{\sigma}^2_{\tilde{P}_{f,n}}$ holds true. For this reason, $\sigma^2_{\tilde{P}_{f,n}}$ can be considered as a more appropriate measure of the numerical uncertainty behind the failure probability.

3.1.3. Approximation of the posterior mean and variance of the failure probability

The posterior mean and variance of the failure probability involves two analytically intractable integrals, as defined in Eqs. (17) and (18). In PBAL-LS [30], the posterior mean and upper bound of the posterior variance (Eqs. (13) and (14)) are evaluated by the crude MCS in a sequential manner. Aside from the algorithmic simplicity and wide applicability, one disadvantage of the crude MCS technique is its poor sampling efficiency. In order to partially alleviate the problem, this study employs the variance-amplified importance sampling (VAIS) developed in [36] to numerically approximate the posterior mean and variance of the failure probability. Hereafter, the VAIS method is referred to as standard deviation-amplified importance sampling (SDA-IS) to avoid possible misunderstanding.

The unbiased SDA-IS estimators for $m_{\tilde{P}_{f,n}}$ and $\sigma^2_{\tilde{P}_{f,n}}$ can be given by:

$$\hat{m}_{\tilde{P}_{f,n}} = \frac{1}{N}\sum_{j=1}^{N} \Phi\left(\frac{-m_{\hat{\beta}_n}\left(\boldsymbol{u}^{\perp,(j)}\right)}{\sqrt{1+\sigma^2_{\hat{\beta}_n}\left(\boldsymbol{u}^{\perp,(j)}\right)}}\right) \frac{\phi_{\boldsymbol{U}^{\perp}}(\boldsymbol{u}^{\perp,(j)})}{\phi_{\boldsymbol{U}^{\perp},\lambda}(\boldsymbol{u}^{\perp,(j)})}, \tag{25}$$

$$\hat{\sigma}^2_{\tilde{P}_{f,n}} = \frac{1}{N}\sum_{j=1}^{N} k_{\tilde{\Phi}_n(-\tilde{\beta})}(\boldsymbol{u}^{\perp,(j)}, \boldsymbol{u}^{\perp\prime,(j)}) \frac{\phi_{\boldsymbol{U}^{\perp}}(\boldsymbol{u}^{\perp,(j)})\phi_{\boldsymbol{U}^{\perp}}(\boldsymbol{u}^{\perp\prime,(j)})}{\phi_{\boldsymbol{U}^{\perp},\lambda}(\boldsymbol{u}^{\perp,(j)})\phi_{\boldsymbol{U}^{\perp},\lambda}(\boldsymbol{u}^{\perp\prime,(j)})}, \tag{26}$$

where $\left\{\boldsymbol{u}^{\perp,(j)}\right\}_{j=1}^{N}$ and $\left\{\boldsymbol{u}^{\perp\prime,(j)}\right\}_{j=1}^{N}$ are two sets of N random samples drawn from $\phi_{\boldsymbol{U}^{\perp},\lambda}(\boldsymbol{u}^{\perp})$ and $\phi_{\boldsymbol{U}^{\perp},\lambda}(\boldsymbol{u}^{\perp\prime})$, respectively; $\phi_{\boldsymbol{U}^{\perp},\lambda}(\boldsymbol{u}^{\perp})$ is the IS density of the form $\phi_{\boldsymbol{U}^{\perp},\lambda}(\boldsymbol{u}^{\perp}) = \prod_{i=1}^{d-1}\phi_{U_i^{\perp},\lambda}(u_i^{\perp})$, in which

$$\phi_{U_i^{\perp},\lambda}(u_i^{\perp}) = \frac{1}{\lambda\sqrt{2\pi}}\exp\left(-\frac{u_i^{\perp,2}}{2\lambda^2}\right), \tag{27}$$

where $\lambda > 1$ is the SDA factor.

The variances associated with the above two estimators are expressed as:

$$\mathbb{V}\left[\hat{m}_{\tilde{P}_{f,n}}\right] = \frac{1}{N(N-1)}\sum_{j=1}^{N}\left[\varPhi\left(\frac{-m_{\hat{\beta}_n}\left(\boldsymbol{u}^{\perp,(j)}\right)}{\sqrt{1+\sigma^2_{\hat{\beta}_n}\left(\boldsymbol{u}^{\perp,(j)}\right)}}\right)\frac{\phi_{\boldsymbol{U}^{\perp}}(\boldsymbol{u}^{\perp,(j)})}{\phi_{\boldsymbol{U}^{\perp},\lambda}(\boldsymbol{u}^{\perp,(j)})} - \hat{m}_{\tilde{P}_{f,n}}\right]^2, \tag{28}$$

$$\mathbb{V}\left[\hat{\sigma}^2_{\tilde{P}_{f,n}}\right] = \frac{1}{N(N-1)}\sum_{j=1}^{N}\left[k_{\tilde{\varPhi}_n(-\tilde{\beta})}(\boldsymbol{u}^{\perp,(j)},\boldsymbol{u}^{\perp\prime,(j)})\frac{\phi_{\boldsymbol{U}^{\perp}}(\boldsymbol{u}^{\perp,(j)})\phi_{\boldsymbol{U}^{\perp}}(\boldsymbol{u}^{\perp\prime,(j)})}{\phi_{\boldsymbol{U}^{\perp},\lambda}(\boldsymbol{u}^{\perp,(j)})\phi_{\boldsymbol{U}^{\perp},\lambda}(\boldsymbol{u}^{\perp\prime,(j)})} - \hat{\sigma}^2_{\tilde{P}_{f,n}}\right]^2. \tag{29}$$

Note that even though the SDA-IS method only works with the GP posterior, rather than the typically expensive-to-evaluate β function, it can be relatively time-consuming, especially when approximating the posterior variance due to the necessity of numerically evaluating the bivariate Gaussian CDF. To guarantee the accuracy and efficiency, it is suggested to implement the SDA-IS method in a sequential way. That is, we can sequentially increase the sample size (e.g., 1×10^4, 2×10^4, ...) until the two COVs of the estimators are respectively smaller than the prescribed tolerances δ_1 and δ_2, i.e., $\sqrt{\mathbb{V}\left[\hat{m}_{\tilde{P}_{f,n}}\right]}/\hat{m}_{\tilde{P}_{f,n}} < \delta_1$ and $\sqrt{\mathbb{V}\left[\hat{\sigma}^2_{\tilde{P}_{f,n}}\right]}/\hat{\sigma}^2_{\tilde{P}_{f,n}} < \delta_2$.

3.2. Stopping criterion and learning function

In terms of the second-order statistics, we have so far completed a Bayesian treatment of the failure probability integral defined in Eq. (6). That is, once given data $\boldsymbol{\mathcal{D}} = \left\{\boldsymbol{\mathcal{U}}^{\perp}, \boldsymbol{\mathcal{Y}}\right\}$, we can make Bayesian inference about the failure probability, including the posterior mean and variance. It is noted that $\boldsymbol{\mathcal{U}}^{\perp}$ can be arbitrarily chosen without specified restrictions in theory. The Bayesian interpretation also allows us to frame the failure probability integral estimation in a Bayesian active learning setting, based on the full exploitation of the posterior statistics of the failure probability. This framework consists mainly of a stopping criterion and a learning function.

3.2.1. Stopping criterion

The stopping criterion can be naturally defined based on the estimated posterior COV of the failure probability such that:

$$\widehat{\mathrm{COV}}_{\tilde{P}_{f,n}} = \frac{\hat{\sigma}_{\tilde{P}_{f,n}}}{\hat{m}_{\tilde{P}_{f,n}}} < \eta, \tag{30}$$

where η is a user-defined threshold. As both $\hat{\sigma}_{\tilde{P}_{f,n}}$ and $\hat{m}_{\tilde{P}_{f,n}}$ may process some approximation errors to some extent, Eq. (30) is required to satisfy twice in a row in order to avoid possible fake convergence. Compared

to the upper bound of posterior COV defined in Eq. (16), the posterior COV is a more suitable quality that can measure the extent of variability in relation to the posterior mean of the failure probability. This makes it easier to specify an appropriate threshold for the stopping criterion before running the method.

3.2.2. Learning function

In case that the above stopping criterion is not met, a learning function is needed to suggest the best next point to query the β-function, rather than choosing it arbitrarily. Based on the posterior variance of the failure probability, a new learning function, termed 'posterior standard deviation contribution' (PSDC), is proposed:

$$\mathrm{PSDC}\left(\boldsymbol{u}^{\perp}\right) = \phi_{\boldsymbol{U}^{\perp}}(\boldsymbol{u}^{\perp}) \times \int_{\mathcal{U}^{\perp}} k_{\tilde{\Phi}_n(-\tilde{\beta})}(\boldsymbol{u}^{\perp}, \boldsymbol{u}^{\perp\prime}) \phi_{\boldsymbol{U}^{\perp\prime}}(\boldsymbol{u}^{\perp\prime}) \mathrm{d}\boldsymbol{u}^{\perp\prime}. \tag{31}$$

It is easy to check that $\int_{\mathcal{U}^{\perp}} \mathrm{PSDC}\left(\boldsymbol{u}^{\perp}\right) \mathrm{d}\boldsymbol{u}^{\perp} = \sigma^2_{\tilde{P}_{f,n}}$ holds true. In this respect, the PSDC function can be regarded as a measure of the contribution of the numerical uncertainty at site $\boldsymbol{u}^{\perp}$ to the posterior variance (or rather the posterior standard deviation) of the failure probability. It is worth mentioning that the UPSDC function (Eq. (15)) is actually an upper bound of the proposed PSDC function. Besides, the UPSDC function only includes the posterior variance function of $\Phi(-\beta)$, not the posterior covariance function, which can reveal spatial correlation, while the proposed PSDC does. Therefore, the PSDC function provides a more informative indicator regarding the degree of contribution of a specific realization in the sample space towards the level of epistemic uncertainty associated with the failure probability. By selecting the point maximizing the PSDC function as the best next point to evaluate the β function, it is expected that $\sigma^2_{\tilde{P}_{f,n+1}}$ will be reduced the most. This involves an optimization problem, where one should note that an analytically intractable integral is involved in the objective function (i.e., the PSDC function).

In this study, we propose to approximate the integral term in Eq. (31) by a numerical integration scheme, called unscented transformation [44]. In this context, the PSDC function can be approximated by the following expression:

$$\widehat{\mathrm{PSDC}}\left(\boldsymbol{u}^{\perp}\right) = \phi_{\boldsymbol{U}^{\perp}}(\boldsymbol{u}^{\perp}) \sum_{i=0}^{2(d-1)} w_i k_{\tilde{\Phi}_n(-\tilde{\beta})}(\boldsymbol{u}^{\perp}, \boldsymbol{u}^{\perp\prime,(i)}), \tag{32}$$

where the $2(d-1)+1$ integration points and weights are given by [44]

$$\begin{aligned}
\boldsymbol{u}^{\perp\prime,(0)} &= \mathbf{0}, w_0 = \frac{\varrho}{d-1+\varrho}, \\
\boldsymbol{u}^{\perp\prime,(i)} &= \sqrt{d-1+\varrho}\boldsymbol{e}_i, w_i = \frac{1}{d-1+\varrho}, \\
\boldsymbol{u}^{\perp\prime,(i+d-1)} &= -\sqrt{d-1+\varrho}\boldsymbol{e}_i, w_{i+d-1} = \frac{1}{d-1+\varrho},
\end{aligned} \tag{33}$$

where ϱ is a free parameter specified as $\varrho = (d-1)-3 = d-4$ [44]; $\boldsymbol{e}_i = [0, \cdots, 0, 1, \cdots, 0]$, $i = 1, 2, \cdots, d-1$.

The best next point is identified by maximizing the $\widehat{\text{PSDC}}$ function such that:

$$\boldsymbol{u}^{\perp,(n+1)} = \underset{\boldsymbol{u}^{\perp}\in\mathcal{U}^{\perp}}{\arg\max} \log \widehat{\text{PSDC}}\left(\boldsymbol{u}^{\perp}\right). \tag{34}$$

It should be pointed out that each evaluation of $\widehat{\text{PSDC}}\left(\boldsymbol{u}^{\perp}\right)$ can still be slightly computationally demanding, though the integral involved in the $\text{PSDC}\left(\boldsymbol{u}^{\perp}\right)$ function is approximated by only using $2(d-1)+1$ points. In this work, we apply a commonly-used nature-inspired optimization method, called particle swarm optimization, but other more efficient techniques can also be explored.

Once $\boldsymbol{u}^{\perp,(n+1)}$ is obtained, $y^{(n+1)} = \beta\left(\boldsymbol{u}^{\perp,(n+1)}\right)$ can be evaluated according the method described in the coming subsection. It follows that the previous dataset can be enriched with $\left\{\boldsymbol{u}^{\perp,(n+1)}, y^{(n+1)}\right\}$, and one can make Bayesian inference about the failure probability based on the enriched data.

3.3. Step-by-step procedure of the proposed method

The above two subsections only focus on several important ingredients (e.g., the posterior variance, learning function and stopping criterion), while there are still some aspects left for implementing the proposed method, such as the important direction and evaluation of β function. Due to length limitation, these aspects are directly embedded in the numerical implementation procedure of the proposed method in the following.

The procedure of the proposed BAL-LS method consists of six main steps, as illustrated by the flowchart (Fig. 3) and summarized below:

Step 1: Choosing an initial important direction

The proposed BAL-LS method has to been initialized with an initial important direction $\boldsymbol{\alpha}^{(0)}$. As suggested in PAL-LS, a convenient choice is the negative normalized gradient of the $\mathcal{G}$-function at the origin

[30]:

$$\boldsymbol{\alpha}^{(0)} = -\frac{\nabla_{\boldsymbol{u}}\mathcal{G}(\mathbf{0})}{||\nabla_{\boldsymbol{u}}\mathcal{G}(\mathbf{0})||}, \tag{35}$$

where $\nabla_{\boldsymbol{u}}\mathcal{G}(\mathbf{0}) = \left[\frac{\partial\mathcal{G}(\mathbf{0})}{\partial u_1}, \frac{\partial\mathcal{G}(\mathbf{0})}{\partial u_2}, \cdots, \frac{\partial\mathcal{G}(\mathbf{0})}{\partial u_d}\right]$; $||\cdot||$ denotes the 2-norm. In case that the gradient information of $\mathcal{G}$ is not available, one can simply apply the numerical differentiation method at the cost of $(d+1)$ $\mathcal{G}$-function evaluations. After that, the corresponding matrix $\boldsymbol{Q}^{(0)}$ that defines the orthogonal hyperplane perpendicular to $\boldsymbol{\alpha}^{(0)}$ can be specified by means of, e.g., the Gram–Schmidt process.

Step 2: Constructing an initial observation dataset and updating the important direction

This step involves generating an initial observation dataset $\boldsymbol{\mathcal{D}}$ from the β function and updating the important direction. First, a small number of samples (say $n_0 = 5$) on the hyperplane orthogonal to $\boldsymbol{\alpha}^{(0)}$ are generated according to $\phi_{\boldsymbol{U}^{\perp},\lambda}(\boldsymbol{u}^{\perp})$ by using the, e.g., Latin hypercube sampling. These samples are denoted as $\tilde{\boldsymbol{\mathcal{U}}}^{\perp} = \left\{\tilde{\boldsymbol{u}}^{\perp,(i)}\right\}_{i=1}^{n_0}$, each of which can form a line parallel to $\boldsymbol{\alpha}^{(0)}$, i.e., $\boldsymbol{\alpha}^{(0)}u^{\parallel} + \boldsymbol{Q}^{(0)}\tilde{\boldsymbol{u}}^{\perp,(i)}$. Second, one has to find the distance between $\tilde{\boldsymbol{u}}^{\perp,(i)}$ and the limit state surface $\mathcal{G} = 0$ along $\boldsymbol{\alpha}^{(0)}$, which is identical to fining the root of $\mathcal{G}\left(\boldsymbol{\alpha}^{(0)}u^{\parallel} + \boldsymbol{Q}^{(0)}\tilde{\boldsymbol{u}}^{\perp,(i)}\right) = 0$. In this study, we develop an adaptive inverse interpolation (AII) method for solving the aforementioned equation. The idea is to use the cubic spline interpolation to approximate the inverse of $\mathcal{G}$ along the direction $\boldsymbol{\alpha}^{(0)}$. To get started, two values $z^{(1)}$ and $z^{(2)}$ of $\mathcal{G}\left(\boldsymbol{\alpha}^{(0)}u^{\parallel} + \boldsymbol{Q}^{(0)}\tilde{\boldsymbol{u}}^{\perp,(i)}\right)$ at two prescribed points (say $u^{\parallel,(1)}$ and $u^{\parallel,(2)}$) are determined. As a convenient rule of thumb, $u^{\parallel,(1)}$ and $u^{\parallel,(2)}$ in this study are set to be 3 and 7, respectively. A rough root (denote as $u^{\parallel,(3)}$) can be found by performing a cubic spline interpolation of the two data points $\left(z^{(1)}, u^{\parallel,(1)}\right)$ and $\left(z^{(2)}, u^{\parallel,(2)}\right)$ at $z = 0$, and the third value $z^{(3)}$ is obtained by evaluating $\mathcal{G}\left(\boldsymbol{\alpha}^{(0)}u^{\parallel,(3)} + \boldsymbol{Q}^{(0)}\tilde{\boldsymbol{u}}^{\perp,(i)}\right)$. One can identify the next approximate root $u^{\parallel,(4)}$ by interpolating the three data points $\left(z^{(1)}, u^{\parallel,(1)}\right)$, $\left(z^{(2)}, u^{\parallel,(2)}\right)$ and $\left(z^{(3)}, u^{\parallel,(3)}\right)$ at $z = 0$. The process is repeated until the relative distance of two consecutive approximate roots is less than a small threshold γ (e.g., 5%), i.e., $\left|u^{\parallel,(j+1)} - u^{\parallel,(j)}\right| / u^{\parallel,(j)} < \gamma$, $j = 3, 4, \cdots$. Typically, the stopping criterion can be reached after several iterations. The final n_0 roots corresponding to $\tilde{\boldsymbol{\mathcal{U}}}^{\perp}$ are denoted as $\tilde{\boldsymbol{\mathcal{Y}}} = \left\{\tilde{y}^{(i)}\right\}_{i=1}^{n_0}$, and each approximate intersection point of the line $\boldsymbol{\alpha}^{(0)}u^{\parallel} + \boldsymbol{Q}^{(0)}\tilde{\boldsymbol{u}}^{\perp,(i)}$ and the limit state surface $\mathcal{G} = 0$ is recorded as $\boldsymbol{\alpha}^{(0)}\tilde{y}^{(i)} + \boldsymbol{Q}^{(0)}\tilde{\boldsymbol{u}}^{\perp,(i)}$. Third, a new important direction $\boldsymbol{\alpha}^{(1)}$ is identified as the normalized vector of the approximate intersection point with the shortest distance to

the origin, and the associated matrix $\boldsymbol{Q}^{(1)}$ can be specified. Fourth, one can obtain the initial observation dataset $\mathcal{D} = \left\{\boldsymbol{\mathcal{U}}^{\perp}, \boldsymbol{\mathcal{Y}}\right\}$ simply by projecting those n_0 approximate intersection points on the hyperplane orthogonal to $\boldsymbol{\alpha}^{(1)}$. Let $n = n_0$ and $q = 1$. It is worth mentioning that one does not need to re-evaluate the $\mathcal{G}$ function, though the important direction is changed in this step. For a schematic illustration of this step, one can refer to Fig. 2.

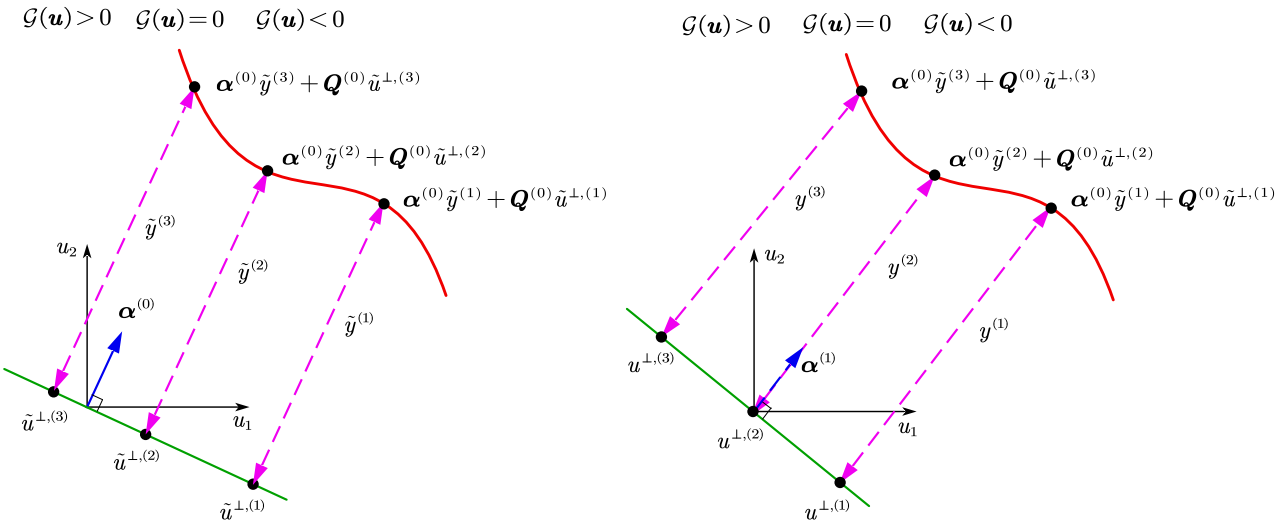

(a) Before changing important direction

(b) After changing important direction

Figure 2: Schematic illustration of Step 2 of the proposed BAL-LS algorithm in two dimensions ($n_0 = 3$).

Step 3: Making Bayesian inference about the failure probability

Conditional on the observation dataset $\mathcal{D}$, the posterior mean and variance of the failure probability can be inferred. To do so, the posterior mean and covariance functions of the β-function are first obtained by Eqs. (11) and (12), and this task can be done by using the *fitrgp* function in Statistics and Machine Learning Toolbox of Matlab. In this study, the prior mean function is assumed to be a constant value and the prior covariance function adopts the squared exponential kernel with a separate length scale per dimension. The hyper-parameters are determined by the maximum likelihood estimation. The posterior mean and variance estimates of the failure probability are then computed by the SDA-IS method in a sequential manner, as described in section 3.1.3. The SDA factor λ is set to be 1.5, and two tolerances δ_1 and δ_2 are specified as 1% and 10%, respectively.

Step 4: Checking the stopping criterion

If the stopping criterion given in Eq. (30) is satisfied twice in a row, then go to **Step 5**. Otherwise, go to **Step 6**. In this study, the associated threshold η is taken as 5%.

Step 5: Enriching the observation dataset and updating the important direction

The best next point $\tilde{\boldsymbol{u}}^{\perp,(n+1)}$ to evaluate the β-function is identified by maximizing the proposed $\widehat{\text{PSDC}}$ function, according to Eq. (34). The β-function value $\tilde{y}^{(n+1)}$ at $\tilde{\boldsymbol{u}}^{\perp,(n+1)}$ can be obtained by solving the equation $\mathcal{G}\left(\boldsymbol{\alpha}^{(q)}u^{\parallel}+\boldsymbol{Q}^{(q)}\tilde{\boldsymbol{u}}^{\perp,(n+1)}\right)=0$. Different from **Step 2**, the Newton's method is used here with a starting point taken as $m_{\tilde{\beta}_n}\left(\tilde{\boldsymbol{u}}^{\perp,(n+1)}\right)$ [30]. Once $\tilde{y}^{(n+1)}$ is solved, a new approximate intersection point $\boldsymbol{\alpha}^{(q)}\tilde{y}^{(n+1)}+\boldsymbol{Q}^{(q)}\tilde{\boldsymbol{u}}^{\perp,(n+1)}$ is available. As long as the new point is the nearest to the origin among all the $n+1$ intersection points, the important direction is updated to $\boldsymbol{\alpha}^{(q+1)}=\left(\boldsymbol{\alpha}^{(q)}\tilde{y}^{(n+1)}+\boldsymbol{Q}^{(q)}\tilde{\boldsymbol{u}}^{\perp,(n+1)}\right)/||\boldsymbol{\alpha}^{(q)}\tilde{y}^{(n+1)}+\boldsymbol{Q}^{(q)}\tilde{\boldsymbol{u}}^{\perp,(n+1)}||$. After that, a new matrix $\boldsymbol{Q}^{(q+1)}$ can be specified. The enriched observation dataset can be obtained by projecting the $n+1$ intersection points on the latest hyperplane orthogonal to $\boldsymbol{\alpha}^{(q+1)}$ and let $q=q+1$. Otherwise, one can simply enrich the previous dataset with $(\tilde{\boldsymbol{u}}^{\perp,(n+1)},\tilde{y}^{(n+1)})$. Let $n=n+1$ and go to **Step 3**.

Step 6: Ending the algorithm

Return the last posterior mean estimate of the failure probability and end the algorithm.

4. Numerical examples

The performance of the proposed BAL-LS method is demonstrated in this section by means of four numerical examples. The reference result of the failure probability for each example is produced by the crude MCS method with a sufficiently large sample size when applicable. For comparison purposes, we also implement several existing methods, including sequential quadratic programming (SQP) based FORM [45] (denoted as FORM-SQP), SORM [12], traditional LS [9], AGPR-LS [35] and PBAL-LS [30]. All methods expcet PBAL-LS are based on the use of FORM-SQP to provide the most probable point (MPP) if applicable. Otherwise, FORM-HLRF [11] is applied instead. For repeatability, the initial points of FORM-SQP and FORM-HLRF are selected as the origin. For traditional LS, the Newton's method is adopted for processing

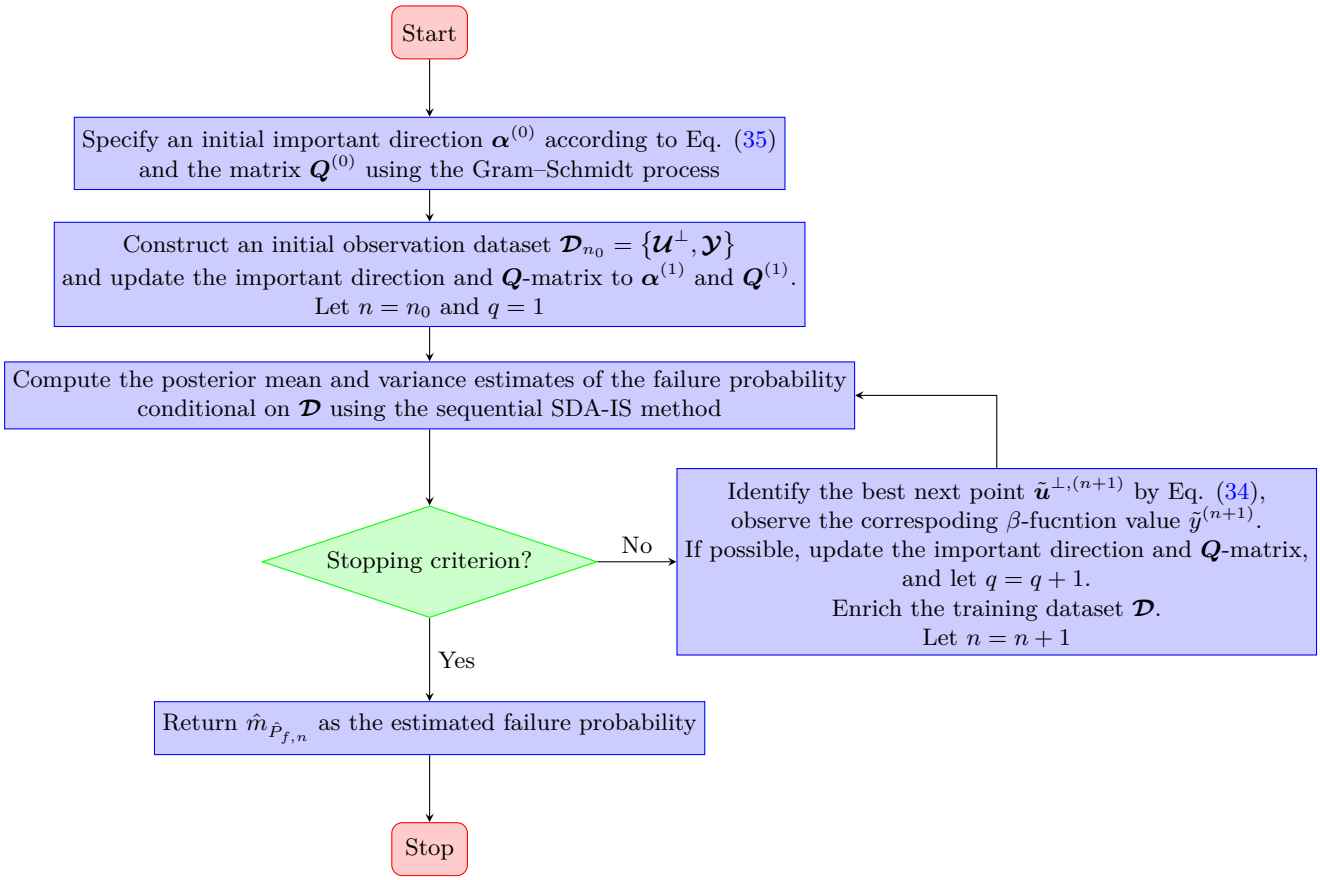

Figure 3: Flowchart of the proposed BAL-LS method.

each line. Similar to the proposed BAL-LS, the stopping criterion in PBAL-LS is also required to meet twice in succession and the tolerance is set to be 5%. Note that even though the gradient information for some numerical examples is easy to solve analytically, we treat them as black-box problems.

4.1. Example 1: A test function

The first numerical example takes a test function of the form [30]:

$$Z = g(\boldsymbol{X}) = a - X_2 + bX_1^3 + c\sin(dX_1), \tag{36}$$

where X_1 and X_2 are two i.i.d. standard normal variables; a, b, c and d are four constant parameters, the values of which are set as $a = 5.5$, $b = 0.02$ and $c = \frac{5}{6}$, $d = \frac{\pi}{3}$.

The reference value of the failure probability is 3.57×10^{-7} (with a COV being 0.53%), which is provided by MCS with 10^{11} samples. The proposed method is compared to several other methods, as summarized

in Table 2. FORM-SQP only requires 28 performance function evaluations, which, however, produces a poor failure probability estimate. The poor accuracy of FORM-SQP can be significantly improved by using SORM, with 7 additional performance function calls. The traditional LS method is carried out twice with two different numbers of lines (i.e., 100 and 200). In both cases, the traditional LS method is able to yield more accurate results than FORM-SQP, but it requires considerably more computational costs. By using AGPR-LS, PBAL-LS and BAL-LS, the number of lines and performance function calls can be significantly reduced, while maintaining reasonable accuracy. Compared to AGPR-LS and PBAL-LS, the proposed BAL-LS method is more efficient in terms of N_{call}.

Table 2: Results for Example 1 by several different methods.

Method	$\hat{P}_f$	$\delta_{\hat{P}_f}$ or $\overline{\delta}_{\hat{P}_f}$	N_{line}	N_{total}
MCS	3.57×10^{-7}	0.53%	-	10^{11}
FORM-SQP	7.19×10^{-7}	-	-	28
SORM	3.53×10^{-7}	-	-	35
Traditional LS	3.36×10^{-7}	7.56%	100	376
	3.70×10^{-7}	4.66%	200	706
AGPR-LS	3.63×10^{-7}	2.24%	10	46
PBAL-LS	3.56×10^{-7}	1.60%	14	40
Proposed BAL-LS	3.56×10^{-7}	3.40%	8	30

Note: $\hat{P}_f$ = failure probability estimate; $\delta_{\hat{P}_f}$ = COV of $\hat{P}_f$; $\overline{\delta}_{\hat{P}_f}$ = upper bound of the COV of $\hat{P}_f$, which is only used for PBAL-LS; N_{line} = the number of lines; N_{total} = the total number of performance function calls.

For illustration purposes, Fig. 4 shows some computational details of the proposed BAL-LS method, including the initial and final importance directions, and approximate intersections points. It can be seen

that the initial importance direction given by Eq. (35) is far from optimal, while the final one is almost optimal. This indicates the effectiveness of the proposed learning function for suggesting next best points to query, as well as the developed strategy for automatically updating the importance direction. What is more, those approximate intersection points are very close to the true limit state line, implying the accuracy of the proposed line search algorithm.

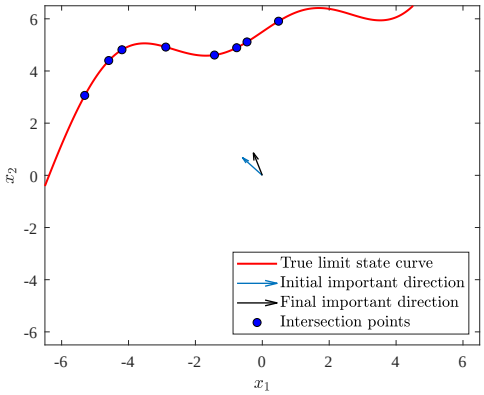

Figure 4: Illustration of the proposed BAL-LS method for Example 1.

4.2. Example 2: A nonlinear oscillator

A nonlinear single-degree-of-freedom (SDOF) oscillator under a rectangular pulse load [46] is considered as a second example, which is shown in Fig. 5. The limit state function is given by:

$$Z = g\left(m, k_1, k_2, r, F_1, t_1\right) = 3r - \left| \frac{2F_1}{k_1 + k_2} \sin\left(\frac{t_1}{2} \sqrt{\frac{k_1 + k_2}{m}} \right) \right|, \tag{37}$$

where m, k_1, k_2, r, F_1 and t_1 are six random variables, as listed in Table 3.

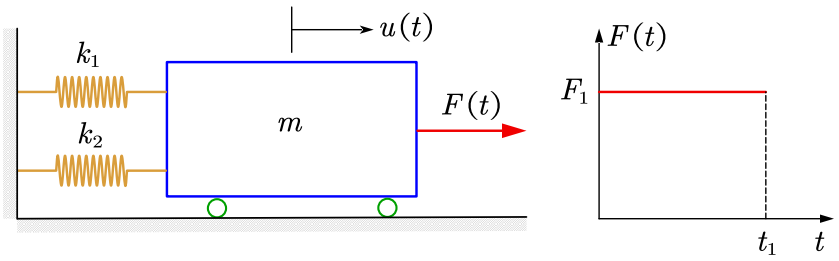

Figure 5: A nonlinear SDOF oscillator driven by a rectangular pulse load.

Table 3: Random variables for Example 2.

Variable	Description	Distribution	Mean	COV
m	Mass	Lognormal	1.0	0.05
k_1	Stiffness	Lognormal	1.0	0.10
k_2	Stiffness	Lognormal	0.2	0.10
r	Yield displacement	Lognormal	0.5	0.10
F_1	Load amplitude	Lognormal	0.4	0.20
t_1	Load duration	Lognormal	1.0	0.20

A reference solution to the failure probability is obtained as 4.01×10^{-8} (with a COV being 0.50%), generated by MCS with 10^{12} samples. The proposed BAL-LS method is conducted to assess the failure probability, as well as several other methods, i.e., FORM-SQP, SORM, traditional LS, AGPR-LS and PBAL-LS. The key results of these methods are summarized in Table 4. Similar to the first example, FORM-SQP still produces an inaccurate failure probability estimate (i.e., 4.88×10^{-8}) even at the cost of 176 $\mathcal{G}$-function evaluations in this example. With more calls to the $\mathcal{G}$-function, SORM can produce an accurate failure probability estimate, say 4.08×10^{-8}. The traditional LS method can improve the accuracy of FORM-SQP by using a number of additional lines to probe the failure domain, which in turn leads to the significant increase in computational costs. AGPR-LS, PBAL-LS and BAL-LS are able to produce failure probability estimates with desirable accuracy. Among them, AGPR-LS requires the most performance function calls (say 205), while the proposed BAL-LS method requires the fewest (say 39).

4.3. Example 3: A reinforced concrete section

For the third example, we consider the bending limit state of a reinforced concrete section [47, 48], as shown in Fig. 6. The limit state function is expressed as:

$$Z = g(\boldsymbol{X}) = X_1 X_2 X_3 - \frac{X_1^2 X_2^2 X_4}{X_5 X_6} - X_7, \tag{38}$$

where X_1 to X_7 are seven basic random variables, as detailed in Table 5.

Table 4: Results for Example 2 by several different methods.

Method	$\hat{P}_f$	$\delta_{\hat{P}_f}$ or $\overline{\delta}_{\hat{P}_f}$	N_{line}	N_{total}
MCS	4.01×10^{-8}	0.50%	-	10^{12}
FORM-SQP	4.88×10^{-8}	-	-	176
SORM	4.08×10^{-8}	-	-	219
Traditional LS	4.22×10^{-8}	2.83%	50	376
	4.09×10^{-8}	2.10%	100	576
AGPR-LS	3.93×10^{-8}	0.81%	21	205
PBAL-LS	4.14×10^{-8}	3.76%	22	62
Proposed BAL-LS	4.07×10^{-8}	1.13%	13	39

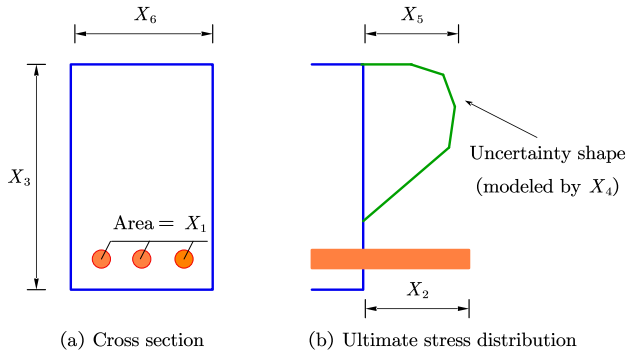

Figure 6: Ultimate stress state for the reinforced concrete section.

As indicated by the reference result from the crude MCS method, this example also constitutes a situation where the probability of failure is extremely small, say 1.57×10^{-8}. Table 6 reports the main results of several selected methods. As seen, the failure probability estimate given by FORM-SQP is less accurate; however, it requires a total number of 157 $\mathcal{G}$-function calls. With 214 $\mathcal{G}$-function calls, SORM gives a less accurate value of the failure probability estimate, say 1.44×10^{-8}. The accuracy of FORM-SQP can be further improved by the traditional LS method by generating additional lines, which leads to increased $\mathcal{G}$-function evaluations at the same time. AGPR-LS is able to provide an accurate failure probability estimate with 8 additional lines, while relying on the MPP provided by FORM-SQP, which requires 157 additional

Table 5: Basic random variables for Example 3.

Variable	Description	Distribution	Mean	COV
X_1	Area of reinforcement	Normal	1260 mm^2	0.05
X_2	Yield stress of reinforcement	Lognormal	300 N/mm^2	0.10
X_3	Effective depth of reinforcement	Normal	770 mm	0.05
X_4	Stress–strain factor of concrete	Lognormal	0.35	0.10
X_5	Compressive strength of concrete	Lognormal	30 N/mm^2	0.15
X_6	Width of section	Normal	400 mm	0.05
X_7	Applied bending moment	Lognormal	80 kN·m	0.20

calls to the $\mathcal{G}$-function. Both PBAL-LS and BAL-LS can give desirable results, but BAL-LS requires less lines and $\mathcal{G}$-function calls.

Table 6: Results for Example 3 by several different methods.

Method	$\hat{P}_f$	$\delta_{\hat{P}_f}$ or $\overline{\delta}_{\hat{P}_f}$	N_{line}	N_{total}
MCS	1.57×10^{-8}	2.53%	-	10^{11}
FORM-SQP	1.46×10^{-8}	-	-	157
SORM	1.44×10^{-8}	-	-	214
Traditional LS	1.59×10^{-8}	1.63%	10	164
	1.59×10^{-8}	1.43%	20	204
AGPR-LS	1.53×10^{-8}	0.54%	8	173
PBAL-LS	1.58×10^{-8}	3.72%	15	55
Proposed BAL-LS	1.58×10^{-8}	0.21%	12	40

4.4. Example 4: A transmission tower structure

The last example consists of a transmission tower structure subject to horizontal and oblique loads, as shown in Fig. 7. Using OpenSees [49], the structure is modeled as a three-dimensional truss with 41 nodes

and 148 elements. The geometric dimensions of the model are marked in Fig. 7 (a) and (b). The limit state function is defined by:

$$Z = g(\boldsymbol{X}) = \Delta - H_1(F_1, F_2, F_3, F_4, F_5, \theta_1, \theta_2, \theta_3, \theta_4, E, A), \tag{39}$$

where Δ denotes a threshold, specified as 50 mm; H_1 represents the horizontal displacement on x-axis of the top node, which is a function of 11 random variables as given in Table 7.

Table 7: Basic random variables for Example 4.

Variable	Description	Distribution	Mean	STD
F_1	Oblique load (in xz - plane)	Lognormal	50 kN	10 kN
F_2	Oblique load (in xz - plane)	Lognormal	50 kN	10 kN
F_3	Oblique load (in xz - plane)	Lognormal	60 kN	12 kN
F_4	Oblique load (in xz - plane)	Lognormal	60 kN	12 kN
F_5	Horizontal load (on x-axis)	Lognormal	80 kN	16 kN
θ_1	Angle	Normal	0°	10°
θ_2	Angle	Normal	0°	10°
θ_3	Angle	Normal	0°	10°
θ_4	Angle	Normal	0°	10°
E	Young's modulus	Normal	200 MPa	30 Mpa
A	Sectional area	Normal	8000 mm^2	800 mm^2

The crude MCS method is not likely to be affordable for providing a reference solution in this example. For this reason, we implement important sampling (IS) [50] as an alternative. The failure probability given by IS is 6.04×10^{-6} with a COV being 1.00%. In this example, FORM-SQP does not converge to the correct result, while FORM-HLRF does. The results from IS, FORM-HLRF, SORM, traditional LS, AGPR-LS, PBAL-LS and BAL-LS are reported in Table 8. Both FORM-HLRF and SORM give inaccurate failure probability estimates. Traditional LS can improve the accuracy of FORM-HLRF by employing additional lines to probe the failure domain, while requiring many additional $\mathcal{G}$-function evaluations in order to provide

a reliable result. AGPR-LS is able to enhance the accuracy of FORM-HLRF, at the cost of many additional computational efforts. PBAL-LS and BALL give reasonably good estimates of the probability of failure. However, BAL-LS is much more efficient than PBAL-LS in this example.

Table 8: Results for Example 4 by several different methods.

Method	$\hat{P}_f$	$\delta_{\hat{P}_f}$ or $\overline{\delta}_{\hat{P}_f}$	N_{line}	N_{total}
IS	6.04×10^{-6}	1.00%	-	64,687
FORM-HLRF	4.19×10^{-6}	-	-	288
SORM	4.33×10^{-6}	-	-	421
Traditional LS	5.86×10^{-6}	5.74%	100	810
	6.16×10^{-6}	3.89%	200	1356
AGPR-LS	6.24×10^{-8}	3.49%	172	468
PBAL-LS	5.86×10^{-6}	4.88%	89	272
Proposed BAL-LS	5.95×10^{-6}	4.65%	23	106

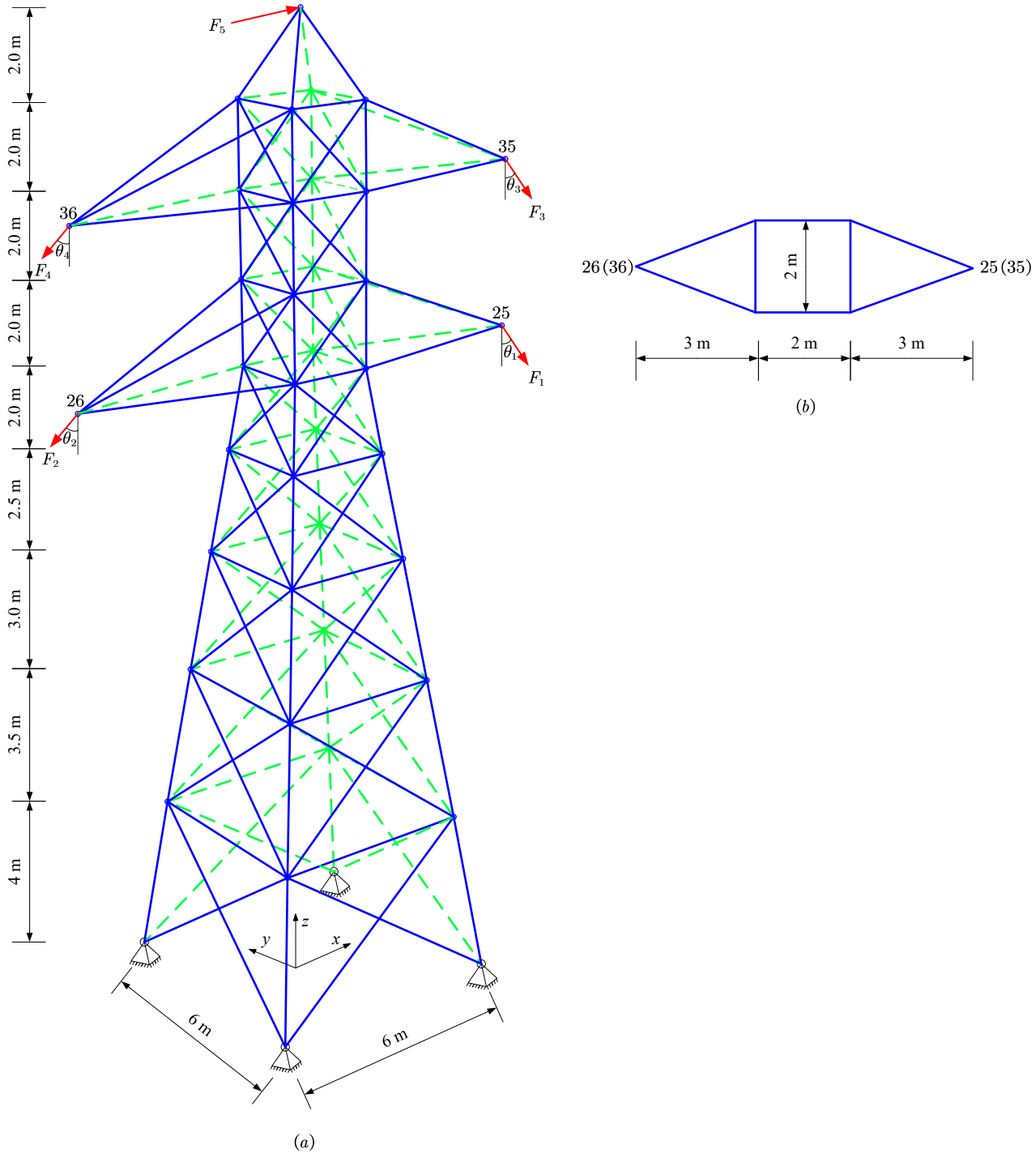

Figure 7: A transmission tower structure subject to horizontal and oblique loads.

5. Concluding remarks

This paper offers a more complete Bayesian active learning treatment of line sampling in the context of structural reliability analysis. This treatment leads to a new method, called 'Bayesian active learning line sampling' (BAL-LS). In this method, we first complete a Bayesian treatment of the standard line sampling in terms of the second-order posterior statistics. Specially, the posterior variance of the failure probability defined in line sampling is derived, which can measure our epistemic uncertainty about the failure probability resulted from a limited number of observations. Then, the Bayesian active learning treatment is accomplished by proposing a learning function and a stopping criterion based on the posterior statistics of the failure probability. Besides, the proposed method can automatically update the importance direction throughout its course without re-evaluating the performance function. From several numerical studies, it is shown that the proposed BAL-LS method is able to assess extremely small failure probabilities for weakly and moderately nonlinear reliability problems with high efficiency and accuracy. Moreover, BAL-LS exhibits a superior performance when compared with our previously developed PBAL-LS in the studied examples.

The proposed method is only suitable for a class of weakly to moderately nonlinear problems in low to moderate dimensions (<20). For highly nonlinear problems, the failure domain can be quite complex in geometry, far from being half-open. The Bayesian active learning framework based on the GP model in its current form can be quite challenging in high dimensions. These limitations can be addressed in future work.

Declaration of competing interest

The authors declare that they have no known competing financial interests or personal relationships that could have appeared to influence the work reported in this paper.

Acknowledgments

Chao Dang is mainly supported by China Scholarship Council (CSC). Jingwen Song would like to acknowledge financial support from the National Natural Science Foundation of China (grant no. 12202358

and 12220101002). Pengfei Wei is grateful to the support from the National Natural Science Foundation of China (grant no. 72171194). Michael Beer would like to thank the support of the National Natural Science Foundation of China under grant number 72271025.

Data availability

Data will be made available on request.

References

[1] C. Dang, P. Wei, M. G. Faes, M. A. Valdebenito, M. Beer, Parallel adaptive Bayesian quadrature for rare event estimation, Reliability Engineering & System Safety (2022) 108621doi:https://doi.org/10.1016/j.ress.2022.108621.

[2] R. Y. Rubinstein, D. P. Kroese, Simulation and the Monte Carlo method, John Wiley & Sons, 2016.

[3] S.-K. Au, J. L. Beck, A new adaptive importance sampling scheme for reliability calculations, Structural Safety 21 (2) (1999) 135–158. doi:https://doi.org/10.1016/S0167-4730(99)00014-4.

[4] N. Kurtz, J. Song, Cross-entropy-based adaptive importance sampling using gaussian mixture, Structural Safety 42 (2013) 35–44. doi:https://doi.org/10.1016/j.strusafe.2013.01.006.

[5] O. Ditlevsen, R. E. Melchers, H. Gluver, General multi-dimensional probability integration by directional simulation, Computers & Structures 36 (2) (1990) 355–368. doi:https://doi.org/10.1016/0045-7949(90)90134-N.

[6] J. Nie, B. R. Ellingwood, Directional methods for structural reliability analysis, Structural Safety 22 (3) (2000) 233–249. doi:https://doi.org/10.1016/S0167-4730(00)00014-X.

[7] S.-K. Au, J. L. Beck, Estimation of small failure probabilities in high dimensions by subset simulation, Probabilistic Engineering Mechanics 16 (4) (2001) 263–277. doi:https://doi.org/10.1016/S0266-8920(01)00019-4.

[8] S.-K. Au, Y. Wang, Engineering risk assessment with subset simulation, John Wiley & Sons, 2014.

[9] P.-S. Koutsourelakis, H. J. Pradlwarter, G. I. Schueller, Reliability of structures in high dimensions, part i: algorithms and applications, Probabilistic Engineering Mechanics 19 (4) (2004) 409–417. doi:https://doi.org/10.1016/j.probengmech.2004.05.001.

[10] P.-S. Koutsourelakis, Reliability of structures in high dimensions. part ii. theoretical validation, Probabilistic Engineering Mechanics 19 (4) (2004) 419–423. doi:https://doi.org/10.1016/j.probengmech.2004.05.002.

[11] A. M. Hasofer, N. C. Lind, Exact and invariant second-moment code format, Journal of the Engineering Mechanics division 100 (1) (1974) 111–121. doi:https://doi.org/10.1061/JMCEA3.0001848.

[12] K. Breitung, Asymptotic approximations for multinormal integrals, Journal of Engineering Mechanics 110 (3) (1984) 357–366. doi:https://doi.org/10.1061/(ASCE)0733-9399(1984)110:3(357).

[13] Y.-G. Zhao, T. Ono, Moment methods for structural reliability, Structural Safety 23 (1) (2001) 47–75. doi:https://doi.org/10.1016/S0167-4730(00)00027-8.

[14] Y.-G. Zhao, Z.-H. Lu, Structural reliability: approaches from perspectives of statistical moments, John Wiley & Sons, 2021.

[15] X. Zhang, M. D. Pandey, Structural reliability analysis based on the concepts of entropy, fractional moment and dimensional reduction method, Structural Safety 43 (2013) 28–40. doi:https://doi.org/10.1016/j.strusafe.2013.03.001.

[16] C. Dang, J. Xu, A mixture distribution with fractional moments for efficient seismic reliability analysis of nonlinear structures, Engineering Structures 208 (2020) 109912. doi:https://doi.org/10.1016/j.engstruct.2019.109912.

[17] C. Ding, C. Dang, M. A. Valdebenito, M. G. Faes, M. Broggi, M. Beer, First-passage probability estimation of high-dimensional nonlinear stochastic dynamic systems by a fractional moments-based mixture distribution approach, Mechanical Systems and Signal Processing 185 (2023) 109775. doi:https://doi.org/10.1016/j.ymssp.2022.109775.

[18] J. Li, J.-B. Chen, Dynamic response and reliability analysis of structures with uncertain parameters, International Journal for Numerical Methods in Engineering 62 (2) (2005) 289–315. doi:https://doi.org/10.1002/nme.1204.

[19] J.-B. Chen, J. Li, Dynamic response and reliability analysis of non-linear stochastic structures, Probabilistic Engineering Mechanics 20 (1) (2005) 33–44. doi:https://doi.org/10.1016/j.probengmech.2004.05.006.

[20] X. Li, G. Chen, H. Cui, D. Yang, Direct probability integral method for static and dynamic reliability analysis of structures with complicated performance functions, Computer Methods in Applied Mechanics and Engineering 374 (2021) 113583. doi:https://doi.org/10.1016/j.cma.2020.113583.

[21] G. Chen, D. Yang, A unified analysis framework of static and dynamic structural reliabilities based on direct probability integral method, Mechanical Systems and Signal Processing 158 (2021) 107783. doi:https://doi.org/10.1016/j.ymssp.2021.107783.

[22] B. J. Bichon, M. S. Eldred, L. P. Swiler, S. Mahadevan, J. M. McFarland, Efficient global reliability analysis for nonlinear implicit performance functions, AIAA Journal 46 (10) (2008) 2459–2468. doi:https://doi.org/10.2514/1.34321.

[23] B. Echard, N. Gayton, M. Lemaire, AK-MCS: an active learning reliability method combining Kriging and Monte Carlo simulation, Structural Safety 33 (2) (2011) 145–154. doi:https://doi.org/10.1016/j.strusafe.2011.01.002.

[24] R. Teixeira, M. Nogal, A. O'Connor, Adaptive approaches in metamodel-based reliability analysis: A review, Structural Safety 89 (2021) 102019. doi:https://doi.org/10.1016/j.strusafe.2020.102019.

[25] M. Moustapha, S. Marelli, B. Sudret, Active learning for structural reliability: Survey, general framework and benchmark, Structural Safety 96 (2022) 102174. doi:https://doi.org/10.1016/j.strusafe.2021.102174.

[26] M. Pellissetti, G. Schuëller, H. Pradlwarter, A. Calvi, S. Fransen, M. Klein, Reliability analysis of spacecraft structures under static and dynamic loading, Computers & Structures 84 (21) (2006) 1313–1325. doi:https://doi.org/10.1016/j.compstruc.2006.03.009.

[27] H. Pradlwarter, G. I. Schueller, P.-S. Koutsourelakis, D. C. Charmpis, Application of line sampling simulation method

to reliability benchmark problems, Structural Safety 29 (3) (2007) 208–221. doi:https://doi.org/10.1016/j.strusafe.2006.07.009.

[28] S. Shufang, L. Zhenzhou, Z. Weiwei, Y. Zhengyin, Reliability and sensitivity analysis of transonic flutter using improved line sampling technique, Chinese Journal of Aeronautics 22 (5) (2009) 513–519. doi:https://doi.org/10.1016/S1000-9361(08)60134-X.

[29] J. Wang, L. S. Katafygiotis, Z. Feng, An efficient simulation method for the first excursion problem of linear structures subjected to stochastic wind loads, Computers & Structures 166 (2016) 75–84. doi:https://doi.org/10.1016/j.compstruc.2016.01.007.

[30] C. Dang, M. A. Valdebenito, J. Song, P. Wei, M. Beer, Estimation of small failure probabilities by partially bayesian active learning line sampling: Theory and algorithm, Computer Methods in Applied Mechanics and Engineering (Under Review).

[31] M. de Angelis, E. Patelli, M. Beer, Advanced line sampling for efficient robust reliability analysis, Structural Safety 52 (2015) 170–182. doi:https://doi.org/10.1016/j.strusafe.2014.10.002.

[32] M. A. Shayanfar, M. A. Barkhordari, M. Barkhori, M. Rakhshanimehr, An adaptive line sampling method for reliability analysis, Iranian Journal of Science and Technology, Transactions of Civil Engineering 41 (3) (2017) 275–282. doi:https://doi.org/10.1007/s40996-017-0070-3.

[33] I. Papaioannou, D. Straub, Combination line sampling for structural reliability analysis, Structural Safety 88 (2021) 102025. doi:https://doi.org/10.1016/j.strusafe.2020.102025.

[34] I. Depina, T. M. H. Le, G. Fenton, G. Eiksund, Reliability analysis with metamodel line sampling, Structural Safety 60 (2016) 1–15. doi:https://doi.org/10.1016/j.strusafe.2015.12.005.

[35] J. Song, P. Wei, M. Valdebenito, M. Beer, Active learning line sampling for rare event analysis, Mechanical Systems and Signal Processing 147 (2021) 107113. doi:https://doi.org/10.1016/j.ymssp.2020.107113.

[36] C. Dang, M. A. Valdebenito, M. G. Faes, P. Wei, M. Beer, Structural reliability analysis: A Bayesian perspective, Structural Safety 99 (2022) 102259. doi:https://doi.org/10.1016/j.strusafe.2022.102259.

[37] J. Jafari-Asl, S. Ohadi, M. E. A. Ben Seghier, N.-T. Trung, Accurate structural reliability analysis using an improved line-sampling-method-based slime mold algorithm, ASCE-ASME Journal of Risk and Uncertainty in Engineering Systems, Part A: Civil Engineering 7 (2) (2021) 04021015.

[38] M. A. Valdebenito, P. Wei, J. Song, M. Beer, M. Broggi, Failure probability estimation of a class of series systems by multidomain line sampling, Reliability Engineering & System Safety 213 (2021) 107673. doi:https://doi.org/10.1016/j.ress.2021.107673.

[39] E. Zio, N. Pedroni, An optimized line sampling method for the estimation of the failure probability of nuclear passive systems, Reliability Engineering & System Safety 95 (12) (2010) 1300–1313. doi:https://doi.org/10.1016/j.ress.2010.06.007.

[40] C. K. Williams, C. E. Rasmussen, Gaussian processes for machine learning, Vol. 2, MIT press Cambridge, MA, 2006.

[41] B. E. Ellison, Two theorems for inferences about the normal distribution with applications in acceptance sampling, Journal of the American Statistical Association 59 (305) (1964) 89–95. doi:https://doi.org/10.2307/2282860.

[42] A. Genz, Numerical computation of rectangular bivariate and trivariate normal and t probabilities, Statistics and Computing 14 (3) (2004) 251–260. doi:https://doi.org/10.1023/B:STCO.0000035304.20635.31.

[43] H. R. Chai, R. Garnett, Improving quadrature for constrained integrands, in: The 22nd International Conference on Artificial Intelligence and Statistics, PMLR, 2019, pp. 2751–2759.

[44] S. J. Julier, J. K. Uhlmann, New extension of the kalman filter to nonlinear systems, in: Signal processing, sensor fusion, and target recognition VI, Vol. 3068, Spie, 1997, pp. 182–193. doi:https://doi.org/10.1117/12.280797.

[45] P.-L. Liu, A. Der Kiureghian, Optimization algorithms for structural reliability, Structural Safety 9 (3) (1991) 161–177. doi:https://doi.org/10.1016/0167-4730(91)90041-7.

[46] C. G. Bucher, U. Bourgund, A fast and efficient response surface approach for structural reliability problems, Structural Safety 7 (1) (1990) 57–66. doi:https://doi.org/10.1016/0167-4730(90)90012-E.

[47] J. Zhou, A. S. Nowak, Integration formulas to evaluate functions of random variables, Structural Safety 5 (4) (1988) 267–284. doi:https://doi.org/10.1016/0167-4730(88)90028-8.

[48] J. Xu, C. Dang, A new bivariate dimension reduction method for efficient structural reliability analysis, Mechanical Systems and Signal Processing 115 (2019) 281–300. doi:https://doi.org/10.1016/j.ymssp.2018.05.046.

[49] F. McKenna, Opensees: a framework for earthquake engineering simulation, Computing in Science & Engineering 13 (4) (2011) 58–66. doi:https://doi.org/10.1109/MCSE.2011.66.

[50] S. Marelli, R. Schöbi, B. Sudret, UQLab user manual – Structural reliability (Rare event estimation), Tech. rep., Chair of Risk, Safety and Uncertainty Quantification, ETH Zurich, Switzerland, report UQLab-V2.0-107 (2022).